

Neutrino-cooled Accretion Disks around Spinning Black Holes

Wen-xin Chen, Andrei M. Beloborodov¹

*Physics Department and Columbia Astrophysics Laboratory, Columbia University, 538
West 120th Street New York, NY 10027*

ABSTRACT

We calculate the structure of accretion disks around Kerr black holes for accretion rates $\dot{M} = 0.001 - 10M_{\odot} s^{-1}$. Such high- \dot{M} disks are plausible candidates for the central engine of gamma-ray bursts. Our disk model is fully relativistic and treats accurately microphysics of the accreting matter: neutrino emissivity, opacity, electron degeneracy, and nuclear composition. The neutrino-cooled disk forms above a critical accretion rate \dot{M}_{ign} that depends on the black hole spin. The disk has the “ignition” radius r_{ign} where neutrino flux rises dramatically, cooling becomes efficient, and the proton-to-nucleon ratio Y_e drops. Other characteristic radii are r_{α} where most of α -particles are disintegrated, r_{ν} where the disk becomes ν -opaque, and r_{tr} where neutrinos get trapped and advected into the black hole. We find r_{α} , r_{ign} , r_{ν} , r_{tr} and show their dependence on \dot{M} . We discuss the qualitative picture of accretion and present sample numerical models of the disk structure. All neutrino-cooled disks regulate themselves to a characteristic state such that: (1) electrons are mildly degenerate, (2) $Y_e \sim 0.1$, and (3) neutrons dominate the pressure in the disk.

Subject headings: accretion, accretion disks — dense matter — gamma rays: bursts

1. INTRODUCTION

A tight neutron-star binary loses orbital momentum via gravitational radiation and eventually merges, forming a black hole and a transient debris disk with a huge accretion rate, comparable to $M_{\odot} s^{-1}$ (see e.g. Ruffert et al. 1997 for numerical simulations). A similar accretion disk may form inside a collapsing massive star, so called “collapsar” (Woosley 1993; see McFadyen & Woosley 1999 for numerical simulations). In this case the central parts of

¹Also at Astro-Space Center of Lebedev Physical Institute, Profsojuznaja 84/32, Moscow 117810, Russia

the stellar core quickly form a black hole of mass $M \sim 2 - 3M_{\odot}$ that grows through accretion on the core-collapse timescale ~ 10 s. If the core material has specific angular momentum substantially above GM/c an accretion disk forms with $\dot{M} = 0.01 - 1M_{\odot} s^{-1}$.

Accretion disks are known to be efficient producers of relativistic jets in various sources associated with black holes, including X-ray binaries and quasars. It is reasonable to expect that the hyper-accreting disks in neutron-star mergers and collapsars produce relativistic jets as well. Because of the huge accretion rate, the power of such jets may be enormous. If a fraction $\sim 10^{-3}$ of the accretion power $\dot{M}c^2$ is channelled to a jet, it will create an explosion with energy $\sim 2 \times 10^{51}(M_{\text{acc}}/M_{\odot})$ erg where M_{acc} is the mass accreted through the disk. Hyper-accreting disk therefore provides a plausible mechanism for powerful relativistic explosions observed as gamma-ray bursts (GRBs, see Piran 2004 for a review).

Accretion in the disk is driven by viscous stress $t_{r\phi}$ that may be expressed as $t_{r\phi} = \alpha p$ where p is pressure inside the disk and $\alpha < 1$ is a dimensionless parameter (Shakura & Sunyaev 1973). Viscous stress is created by magnetic fields that are amplified as a result of magneto-rotational instability. Numerical simulations of this instability show that $\alpha = 0.01 - 0.1$ (see Balbus & Hawley 1998 for a review). In this respect, the hyper-accreting disk is expected to be similar to normal accretion disks in X-ray binaries. It is, however, crucially different as regards microphysics of the accreting matter and its cooling. The optical depth to photon scattering is enormous and radiation cannot escape; it is advected by the matter flow into the black hole (or outward by the jet). The only possible cooling mechanism is neutrino emission. Significant neutrino losses occur at high $\dot{M} > 0.01M_{\odot} s^{-1}$, and then almost all the accretion energy is carried away by neutrinos.

In any realistic scenario, the black hole has a significant spin as it forms from rotating matter and further spun up by accretion. The spin is likely to help the jet formation through, e.g. Blandford-Znajek process. It also increases the overall efficiency of accretion from 6% (zero spin $a = 0$) up to 42% (maximum spin $a = 1$). The black-hole spin has significant effects on the accretion disk because it changes dramatically the spacetime metric near the black hole, where most of accretion power is released. For example, in the extreme case of $a = 1$, the inner radius of the disk is reduced by a factor of 6 compared with the Schwarzschild case. This leads to a higher temperature and a much higher neutrino intensity. Therefore, disks around rapidly spinning black holes may create powerful jets via neutrino annihilation above the disk.

The structure of neutrino-cooled disks was investigated in a number of works, and one of them studied accretion onto a spinning Kerr black hole (Popham, Woosley, & Fryer 1999, hereafter PWF). PWF used accurate equations of relativistic hydrodynamics in Kerr spacetime, however, made simplifying assumptions about the state of accreting matter and

its neutrino emission, which later turned out invalid: (1) Electron degeneracy was neglected. The true degeneracy is significant: it strongly suppresses the e^\pm population, changes the equation of state and neutrino emissivity. (2) Neutron-to-proton ratio was not calculated and no distinction was made between neutrons and protons in the calculation of neutrino emissivity. The correct ratio is typically $n_n/n_p \sim 10$, which leads to a strong suppression of neutrino emission. (3) The produced neutrinos were assumed to escape freely. In the case of a Kerr black hole, this assumption breaks at $\dot{M} \gtrsim 0.1M_\odot \text{ s}^{-1}$ — then the disk is opaque for neutrinos in the inner region where most of accretion power is released.

Recent works discussed one or several of these issues. For example, Di Matteo, Perna, & Narayan (2002) focused on the effects of neutrino opacity at high \dot{M} , however neglected degeneracy and assumed $n_n/n_p = 1$. Kohri & Mineshige (2002) studied strongly degenerate disks, and Kohri, Narayan, & Piran (2005) — the realistic mildly degenerate disks. None of these works, however, attempted the construction of an accretion model in Kerr space-time — all assumed a non-rotating black hole and used a Newtonian or pseudo-Newtonian approximation. Pruet, Woosley, & Hoffman (2003) studied the Kerr disk models of PWF and pointed out that the disk must be neutron rich in the inner region, however did not attempt to model self-consistently the disk structure. Beloborodov (2003a) showed that β -equilibrium is established in disks with $\dot{M} \gtrsim 10^{31}(\alpha/0.1)^{9/5}(M/M_\odot)^{6/5} \text{ g s}^{-1}$, where M is the black hole mass. The relation between temperature, density, and neutron richness in equilibrium was studied in that work, and the disk was shown to become neutron rich in the inner region if $\dot{M} \gtrsim 10^{31}(\alpha/0.1)(M/M_\odot)^2 \text{ g s}^{-1}$. The structure of the disk was not, however, calculated.

In the present paper we develop a self-consistent, fully relativistic model of accretion disks around Kerr black holes. Our study is limited to steady accretion with constant \dot{M} , which is a good approximation at radii where the accretion timescale is shorter than the evolution timescale of the disk (it may be 1 – 10 s, depending on the concrete scenario of disk formation). The accretion rate is assumed to be constant with radius, $\dot{M}(r) = \text{const}$, neglecting the fraction of \dot{M} that may be lost to a jet. The model employs the customary approximation of one-dimensional hydrodynamics (Shakura & Sunyaev 1973) where the effects of three-dimensional MHD turbulence are described by one viscosity parameter α .

In § 2 we summarize the physics of neutrino-cooled disks, write down the set of relevant equations, and point out where progress is made compared with the previous works. We pay particular attention to the mechanism of cooling that couples to and regulates the state of accreting matter. The method of solution of the disk equations is described in § 3, and the results are presented in § 4. Our conclusions are summarized in § 5.

2. PHYSICS OF NEUTRINO-COOLED DISKS

2.1. Outer Boundary Conditions

Generally, the size of accretion disk is limited by the maximum angular momentum of the flow. We here consider only the region where accretion is quasi-steady, i.e. the accretion timescale is smaller than the evolution timescale of \dot{M} . This sets an effective outer boundary r_{out} which depends on the specific scenario of disk formation. In our models, we choose r_{out} sufficiently far (well outside the neutrino ignition radius) to cover the whole neutrino-cooled region.

Neutrino cooling is negligible outside the ignition radius r_{ign} and the viscously dissipated energy is stored in the accretion flow, which makes the disk thick in the outer region. We choose the disk temperature at r_{out} so that the energy content per baryon approximately equals virial energy $\sim GMm_p/r$ as is generally the case in any advective flow (e.g. Narayan & Yi 1994). The flow is assumed to be initially made of alpha particles at the outer boundary. The calculations will show that the flow completely forgets the boundary conditions as it approaches the ignition radius: α -particles are decomposed into free nucleons, and entropy per baryon and lepton number are regulated to certain values by neutrino emission. This convergence makes the details of advective accretion in the outer region unimportant.

Note also that the thick disk in the outer advective region $r \sim r_{\text{out}}$ may produce a strong outflow, so that the accretion rate \dot{M} decreases with radius. However, even this fact is not so important as long as we are given \dot{M} at $r \gtrsim r_{\text{ign}}$ where the disk becomes relatively thin and \dot{M} remains constant.

2.2. One-dimensional Relativistic Hydrodynamics

The disk is described by vertically averaged quantities such as density ρ , temperature T , pressure P , energy density U , electron chemical potential μ_e , neutrino chemical potential μ_ν , etc. The disk is axially symmetric and steady, so all quantities depend of radius r only and we deal with a one-dimensional problem. The difference between radius in cylindrical and spherical coordinates is neglected as if the disk were geometrically thin. This difference is $(r_{\text{sph}} - r_{\text{cyl}})/r \sim (1/2)(H/r)^2 \ll 1$ where $H(r)$ is half-thickness of the disk at radius r . The thin-disk approximation is quite accurate inside the ignition radius where $H/r \lesssim 0.1 - 0.4$, and less accurate at $r \sim r_{\text{out}}$ where $H/r \sim 0.7 - 0.8$.

The vertically-averaged model is designed to describe most of the disk material, and it may not describe well the “skin” of the disk, especially if viscous heating is not uniform

in the vertical direction. The vertical structure of the disk is governed by the unknown vertical distribution of heating and the vertical neutrino transport (Sawyer 2003). We do not study the vertical structure in this paper and use the simple “one-zone” approximation of the vertically-averaged disk.

The hydrodynamic equations of a relativistic disk express conservation of baryon number, energy, and momentum (angular and radial) in Kerr spacetime (see Beloborodov 1999 for a review). Hereafter we use Boyer-Lindquist coordinates $x^\alpha = (t, r, \theta, \phi)$ with the corresponding Kerr metric $g_{\alpha\beta}$, which has two parameters: the black hole mass M and its dimensionless spin parameter $0 < a < 1$ (see e.g. Misner, Thorne, & Wheeler 1973). The disk is in the equatorial plane $\theta = \pi/2$ and the fluid motion is described by the four-velocity $u^\alpha = dx^\alpha/d\tau = (u^t, u^r, 0, u^\phi)$, where τ is the proper time of the fluid. The equation of baryon conservation reads

$$u^r = -\frac{\dot{M}}{4\pi r H \rho}, \quad (1)$$

where the half thickness H is to be determined below by the equation of hydrostatic balance.

The exact differential equations of azimuthal and radial motion may be replaced by much simpler and sufficiently accurate conditions following Shakura & Sunyaev (1973) and Page & Thorne (1974). This “thin-disk” approximation neglects terms $\sim (H/r)^2$ and assumes that the fluid is in Keplerian rotation with angular velocity,

$$\Omega = \frac{u^\phi}{u^t} = \Omega_K = \left[\left(\frac{r^3}{GM} \right)^{1/2} + a \frac{GM}{c^3} \right]^{-1}. \quad (2)$$

A small radial velocity is superimposed on this rotation,

$$u^r = -\frac{\alpha}{S} c_s \left(\frac{H}{r} \right), \quad (3)$$

where $c_s = (P/\rho)^{1/2}$ is the isothermal sound speed and $S(r)$ is a numerical factor. This factor is determined by the inner boundary condition (zero torque at the last stable orbit r_{ms}) and the Kerr metric; it is calculated in Appendix A. The accuracy of the thin-disk approximation is not perfect at large radii $r \sim r_{\text{out}}$, where the disk is thick. However, the details of the outer region have no effect on the solution for the neutrino-cooled disk.

The equation of energy conservation reads

$$F^+ - F^- = u^r \left[\frac{d(UH)}{dr} - \frac{(U + P)}{\rho} \frac{d(\rho H)}{dr} \right], \quad (4)$$

where F^+ and F^- are the rates of viscous heating and cooling per unit area of the disk, as measured by the local observer corotating with the disk. F^- depends on the state of the

disk matter that will be discussed in § 2.3 below. F^+ may be expressed in terms of Ω and the kinematic viscosity coefficient ν ,

$$F^+ = \nu H (U + P) g^{rr} g_{\phi\phi} (-g^{tt}) \gamma^4 \left(\frac{d\Omega}{dr} \right)^2, \quad (5)$$

where $\gamma = (-g^{tt})^{-1/2} u^t$ is the Lorentz factor of fluid measured in the frame of a local observer with zero angular momentum. The viscosity coefficient is related to the disk thickness H , sound speed c_s , and α by $\nu = (2/3)\alpha c_s H$.

The model described by equations (2), (3), and (4) neglects the effect of the stored energy and pressure on the radial and azimuthal dynamics of the disk, and retains the advected energy in the energy balance. This approximation is reasonable as may be seen from exact hydrodynamical models: the deviation from Keplerian rotation remains small ($\lesssim 10\%$) even when the advection effect dominates in the energy balance (Beloborodov 1998).¹ Then the main effect of advection is the simple storage of energy that is not radiated away ($F^+ - F^- \neq 0$ in eq. 4). It strongly influences pressure and the scale-height of the disk, and hence changes u^r according to equation (3). Equations (2) and (3) remain, however, good approximations.

The vertical balance is given by

$$\left(\frac{H}{r} \right)^{-2} = \frac{J GM \rho}{r P}, \quad (6)$$

where

$$J = \frac{2(r^2 - ar_g \sqrt{2r_g r} + 0.75a^2 r_g^2)}{2r^2 - 3r_g r + ar_g \sqrt{2r_g r}} \quad (7)$$

is the relativistic correction to the tidal force in the Kerr metric, and

$$r_g = \frac{2GM}{c^2}. \quad (8)$$

In contrast to accretion disks in X-ray binaries and AGN, there is one more conservation law that must be taken into account in GRB disks. The lepton number (or, equivalently, the proton-to-baryon ratio Y_e) may change with radius because the neutrino and anti-neutrino fluxes from the disk may not be equal. The conservation of lepton number is expressed by the equation,

$$\frac{1}{H} (\dot{N}_{\bar{\nu}} - \dot{N}_{\nu}) = u^r \left[\frac{\rho}{m_p} \frac{dY_e}{dr} + \frac{d}{dr} (n_{\nu} - n_{\bar{\nu}}) \right], \quad (9)$$

¹A strong reduction of Ω below Ω_K may occur in the limit of a large disk with no cooling. This limit does not apply to GRB disks.

where \dot{N}_ν and $\dot{N}_{\bar{\nu}}$ are the number fluxes of neutrinos and anti-neutrinos per unit area (from one face of the disk), n_ν and $n_{\bar{\nu}}$ are the number densities of neutrinos and anti-neutrinos inside the disk; they become significant when the disk is opaque (see § 2.4 below). Y_e is related to the neutron-to-proton ratio by $Y_e = (n_n/n_p + 1)^{-1}$.

2.3. Microphysics and Thermodynamic Quantities

The disk is made of neutrons, protons, α -particles, electrons, positrons, photons, neutrinos, and anti-neutrinos. The effect of magnetic field on the particle distribution functions may be neglected (see Beloborodov 2003a). The total pressure and energy density are given by

$$P = P_b + P_\gamma + P_{e^-} + P_{e^+} + P_\nu + P_{\bar{\nu}}, \quad (10)$$

$$U = U_b + U_\gamma + U_{e^-} + U_{e^+} + U_\nu + U_{\bar{\nu}}. \quad (11)$$

Here, the baryon pressure and energy density are

$$P_b = \frac{\rho}{m_p} k_B T \left(X_f + \frac{1 - X_f}{4} \right), \quad U_b = \frac{3}{2} P_b, \quad (12)$$

where X_f is the mass fraction of free nucleons and $1 - X_f$ is the mass fraction of α -particles. X_f is found from the equation of nuclear statistical equilibrium (see e.g. Meyer 1994),

$$4.9 \times 10^2 \rho_{10}^{-3/2} T_{10}^{9/4} \exp \left(-\frac{16.4}{T_{10}} \right) = 4 \left[Y_e - \frac{(1 - X_f)}{2} \right] \left[1 - Y_e - \frac{(1 - X_f)}{2} \right] (1 - X_f)^{-1/2}, \quad (13)$$

where $\rho_{10} = \rho/10^{10}$ g cm⁻³ and $T_{10} = T/10^{10}$ K.

The radiation pressure and energy density are

$$P_\gamma = \frac{a_r T^4}{3}, \quad U_\gamma = 3P_\gamma, \quad (14)$$

where $a_r = 7.56 \times 10^{-15}$ erg cm⁻³ K⁻⁴ is the radiation constant.

Electrons are neither non-degenerate nor strongly degenerate, and they are not ultra-relativistic at all radii. Therefore, no asymptotic expansions are valid, and the thermodynamics quantities for e^\pm must be calculated using the exact Fermi-Dirac distribution. The e^\pm pressure and energy density are given by the integrals,

$$P_{e^\pm} = \frac{1}{3} \frac{(m_e c)^3}{\pi^2 \hbar^3} m_e c^2 \int_0^{+\infty} f(\sqrt{p^2 + 1}, \mp \eta_e) \frac{p^4}{\sqrt{p^2 + 1}} dp, \quad (15)$$

$$U_{e^\pm} = \frac{(m_e c)^3}{\pi^2 \hbar^3} m_e c^2 \int_0^{+\infty} f(\sqrt{p^2 + 1}, \mp \eta_e) \sqrt{p^2 + 1} p^2 dp, \quad (16)$$

where $f(E, \eta)$ is the Fermi-Dirac distribution function,

$$f(E, \eta) = \frac{1}{e^{\frac{E}{\theta} - \eta} + 1}, \quad (17)$$

$\theta = kT/m_e c^2$, $\eta = \mu/kT$ is the dimensionless degeneracy parameter, and μ is chemical potential. Since e^\pm are in equilibrium with radiation due to fast reactions $e^+ + e^- \leftrightarrow \gamma + \gamma$, and photons have zero chemical potential, one has the relation $\mu_{e^-} + \mu_{e^+} = 0$. We denote η_{e^-} by η_e and use $\eta_{e^+} = -\eta_e$ in equations (10) and (11). The e^\pm population is then completely described by two parameters: θ and η_e .

The number densities of e^- and e^+ are

$$n_{e^\pm} = \frac{(m_e c)^3}{\pi^2 \hbar^3} \int_0^{+\infty} f(\sqrt{p^2 + 1}, \mp \eta_e) p^2 dp. \quad (18)$$

The disk matter is neutral, which implies

$$n_{e^-} - n_{e^+} = Y_e \frac{\rho}{m_p}. \quad (19)$$

This gives a relation between θ , η_e , ρ , and Y_e .

The contribution of ν and $\bar{\nu}$ to P and U becomes noticeable only in very opaque disks where neutrinos are completely thermalized and described by Fermi-Dirac distributions with chemical potentials μ_ν and $\mu_{\bar{\nu}} = -\mu_\nu$ (see § 2.4.2). U_ν and $U_{\bar{\nu}}$ in the opaque disk are given by equations (27) and (30) below. The corresponding pressures are $P_\nu = U_\nu/3$ and $P_{\bar{\nu}} = U_{\bar{\nu}}/3$.

2.4. Cooling

The cooling of the disk F^- may be written as a sum of three terms,

$$F^- = F_{\text{nuc}} + F_\nu + F_{\bar{\nu}}. \quad (20)$$

Here F_{nuc} describes the consumption of heat by the disintegration of α particles as the flow approaches the black hole,

$$F_{\text{nuc}} = 6.8 \times 10^{28} \rho_{10} \frac{dX_f}{dr} u^r H, \quad (21)$$

where all quantities are expressed in cgs units. This cooling is dominant in an extended region around $100r_g$ where α -particles gradually disintegrate (see § 4 below).

The terms F_ν and $F_{\bar{\nu}}$ represent the cooling due to emission of neutrinos and anti-neutrinos. There are four different channels of neutrino emission (see e.g. Kohri & Mineshige 2002): (1) electron capture onto protons $p + e^- \rightarrow n + \nu$ and positron capture onto neutrons $n + e^+ \rightarrow p + \bar{\nu}$, (2) pair annihilation $e^+ + e^- \rightarrow \nu + \bar{\nu}$, (3) nucleon-nucleon bremsstrahlung $n + n \rightarrow n + n + \nu + \bar{\nu}$, and (4) plasmon decay $\tilde{\gamma} \rightarrow \nu + \bar{\nu}$. The e^\pm capture strongly dominates neutrino emission in GRB disks, and the other three channels may be safely neglected. The e^\pm annihilation into $\nu\bar{\nu}$ makes a small contribution even when electron degeneracy is neglected (PWF). When degeneracy is taken into account, the positron population is suppressed and the reaction rate becomes completely negligible. Bremsstrahlung and plasmon decay are important only at extremely high degeneracy and negligible in GRB disks.

We calculate below F_ν and $F_{\bar{\nu}}$ due to the e^\pm capture onto nucleons. This calculation is different in the transparent and opaque regions of the disk.

2.4.1. Neutrino Emission from ν -transparent Disk

If the disk is transparent to the emitted neutrinos and anti-neutrinos, the emerging neutrino flux equals the vertically integrated emissivity that is found, e.g., in Shapiro & Teukolsky (1983). This gives,

$$F_\nu = H Y_e \frac{\rho}{m_p} K m_e c^2 \int_0^{+\infty} f(E + Q, \eta_e) (E + Q)^2 \left[1 - \frac{1}{(E + Q)^2} \right]^{1/2} E^3 dE, \quad (22)$$

$$F_{\bar{\nu}} = H (1 - Y_e) \frac{\rho}{m_p} K m_e c^2 \int_{Q+1}^{+\infty} f(E - Q, -\eta_e) (E - Q)^2 \left[1 - \frac{1}{(E - Q)^2} \right]^{1/2} E^3 dE. \quad (23)$$

Here $Q = (m_n - m_p)/m_e = 2.53$, $K = 6.5 \times 10^{-4} \text{ s}^{-1}$, and $f(E, \eta)$ is the Fermi-Dirac distribution (eq. 17).

Similarly, one finds the number flux of neutrinos, which will be used in the equation of lepton number conservation,

$$\dot{N}_\nu = H Y_e \frac{\rho}{m_p} K \int_0^{+\infty} f(E + Q, \eta_e) (E + Q)^2 \left[1 - \frac{1}{(E + Q)^2} \right]^{1/2} E^2 dE, \quad (24)$$

$$\dot{N}_{\bar{\nu}} = H (1 - Y_e) \frac{\rho}{m_p} K \int_{Q+1}^{+\infty} f(E - Q, -\eta_e) (E - Q)^2 \left[1 - \frac{1}{(E - Q)^2} \right]^{1/2} E^2 dE. \quad (25)$$

2.4.2. Neutrino Emission from ν -opaque Disk

Inside a ν -opaque disk, neutrinos relax to thermal equilibrium: a detailed balance is established between absorption and emission. Then neutrinos are described by the Fermi-Dirac distribution, and the energy flux of escaping neutrinos may be written as

$$F_\nu = \frac{U_\nu c}{1 + \tau_\nu}, \quad (26)$$

where

$$U_\nu = \frac{(m_e c)^3}{2\pi^2 \hbar^3} m_e c^2 \int_0^{+\infty} f(E, \eta_\nu) E^3 dE \quad (27)$$

is the energy density of thermalized neutrinos inside the disk and τ_ν is the total optical depth seen by ν , including absorption and scattering (the cross sections of relevant processes are given in Appendix B). The chemical potential of neutrinos $\eta_\nu = \mu_\nu/kT$ that appears in equation (27) is related to μ_e , μ_p , and μ_n because the detailed equilibrium $\nu + n \leftrightarrow e^- + p$ is established. The relation $\mu_\nu + \mu_n = \mu_e + \mu_p$ then gives (see Beloborodov 2003a),

$$\eta_e - \eta_\nu = \ln \left(\frac{1 - Y_e}{Y_e} \right) + \frac{Q}{\theta}. \quad (28)$$

When the disk is opaque also for anti-neutrinos, one finds

$$F_{\bar{\nu}} = \frac{U_{\bar{\nu}} c}{1 + \tau_{\bar{\nu}}}, \quad (29)$$

$$U_{\bar{\nu}} = \frac{(m_e c)^3}{2\pi^2 \hbar^3} m_e c^2 \int_0^{+\infty} f(E, -\eta_\nu) E^3 dE, \quad (30)$$

where we have used $\eta_{\bar{\nu}} = -\eta_\nu$.

Finally, the number fluxes of ν and $\bar{\nu}$ that escape the disk are given in the opaque regime by

$$\dot{N}_\nu = \frac{n_\nu c}{(1 + \tau_\nu)}, \quad n_\nu = \frac{(m_e c)^3}{2\pi^2 \hbar^3} \int_0^{+\infty} f(E, \eta_\nu) E^2 dE, \quad (31)$$

$$\dot{N}_{\bar{\nu}} = \frac{n_{\bar{\nu}} c}{(1 + \tau_{\bar{\nu}})}, \quad n_{\bar{\nu}} = \frac{(m_e c)^3}{2\pi^2 \hbar^3} \int_0^{+\infty} f(E, -\eta_\nu) E^2 dE. \quad (32)$$

2.4.3. Transition Between Transparent and Opaque Regions

Two changes happen at the transition to the opaque regime: (1) the probability of direct neutrino escape is reduced as $(1 + \tau_\nu)^{-1}$, and (2) neutrinos get thermalized. Note that

the rates of neutrino scattering and absorption are comparable, and a large optical depth $\tau_\nu \gg 1$ implies that neutrinos are completely reabsorbed in the disk. The neutrino spectrum significantly changes at the transition: it is described by Fermi-Dirac distribution in the opaque region, with a non-zero chemical potential μ_ν . In particular, the mean energy of neutrinos, \bar{E}_ν/kT , changes.

We model the transition using the following approximate method. First we calculate the energy density of neutrinos that would be obtained in the transparent and opaque limits: $U_\nu^{\text{transp}} = F_\nu/c$ from equation (22) and U_ν^{opaque} from equation (27), and define the parameter

$$x = \frac{U_\nu^{\text{transp}}}{U_\nu^{\text{transp}} + U_\nu^{\text{opaque}}}. \quad (33)$$

If the disk is transparent we must find $U_\nu^{\text{transp}} \ll U_\nu^{\text{opaque}}$ (no reabsorption) and $x \rightarrow 0$. If it is opaque, $U_\nu^{\text{transp}} \gg U_\nu^{\text{opaque}}$ (strong reabsorption) and $x \rightarrow 1$. In our calculations, the neutrino flux is approximated by

$$F_\nu = \begin{cases} U_\nu^{\text{transp}} c (1 + \tau_\nu)^{-1} & \text{if } x < \frac{1}{2}, \\ U_\nu^{\text{opaque}} c (1 + \tau_\nu)^{-1} & \text{if } x \geq \frac{1}{2}. \end{cases} \quad (34)$$

This expression is continuous at the transition point $x = 1/2$.

To model the change of \dot{N}_ν at the transition we approximate the mean energy of the emitted neutrinos by

$$\bar{E}_\nu = (1 - x) \frac{F_\nu^{\text{transp}}}{\dot{N}_\nu^{\text{transp}}} + x \frac{F_\nu^{\text{opaque}}}{\dot{N}_\nu^{\text{opaque}}}. \quad (35)$$

Then we define

$$\dot{N}_\nu = \frac{F_\nu}{\bar{E}_\nu}, \quad (36)$$

which smoothly changes across the transition and has the correct limits at $x = 0$ and $x = 1$. Transition to the opaque region for anti-neutrinos is calculated in the same way.

Finally, we note that emission of muon and tau neutrinos is orders of magnitude weaker compared with the emission of electron neutrinos by e^\pm capture reactions. The main emission mechanism of ν_μ and $\bar{\nu}_\mu$ is nucleon-nucleon bremsstrahlung. The corresponding emissivity when nucleons are non-degenerate ($\rho < 10^{14} \text{ g s}^{-1}$) is given by (Thompson, Burrows, & Horvath 2000)

$$\dot{q}_{\nu_\mu \bar{\nu}_\mu} \approx 10^{30} \zeta \rho_{14}^2 \left(\frac{kT}{\text{MeV}} \right)^{5.5} \text{ erg cm}^{-3} \text{ s}^{-1}, \quad (37)$$

where $\zeta \sim 0.1 - 1$ is a numerical factor. At high densities, when nucleons become degenerate, $\dot{q}_{\nu_\mu \bar{\nu}_\mu}$ saturates at about $10^{34} \text{ erg cm}^{-3} \text{ s}^{-1}$. The muon-neutrino emissivity will be found to be well below F^+/H and therefore may be neglected.

2.5. Comparison with Previous Works

Recent works on neutrino-cooled disks assumed a Schwarzschild black hole, and the main advantage of our model is that it is fully relativistic and describes accretion by Kerr black holes. Other advances compared with the most recent work by Kohri et al. (2005) are as follows. (1) Inclusion of the zero-torque boundary condition at the last stable orbit. This has a strong effect on the heating rate F^+ and the radial velocity u^r . The effect of inner boundary is described by the factor $S(r)$, which is much smaller than unity in the hottest region of the disk, $S \sim 0.1$. (2) Advection of heat and lepton number is treated accurately, using the differential equation of radial transport. This is essential since the disk is far from being self-similar and no analytical approximations are valid. The set of equations then becomes more complicated, however, it allows one to calculate the global model of the disk, from the outer advective region to the last stable orbit. (3) The transition to the opaque region is treated accurately. We find that there is only one thermalized neutrino species (electron neutrino), and its chemical potential μ_ν is obtained from the detailed equilibrium rather than assumed to be zero. (4) A corrected cross-section is used for anti-neutrino absorption by protons, which takes into account the proton recoil (see Appendix B). This minor refinement is interesting only in high- \dot{M} disks that produce high-energy neutrinos.

3. METHOD OF SOLUTION

The disk is described by the set of coupled equations most of which are local, i.e. relate local parameters at a given radius. Two equations, however, are differential (eqs. 4 and 9); they state conservation of energy and lepton number and contain advection terms that describe radial transport of energy and Y_e . We therefore have to specify two boundary conditions.

Our outer boundary is outside the neutrino-cooled disk, in the advective region, where neutrino emission may be neglected and matter is dominated by α -particles. So, one of our boundary conditions is $Y_e(r_{\text{out}}) = 0.5$.

As the other boundary condition one may specify any parameter that gives a reasonable approximation to the advection-dominated solution (Narayan, Piran, & Kumar 2001). For example, one could specify a certain value of $(H/r)^2 \sim 1/2$ that is characteristic for advective disks, and calculate all other parameters at r_{out} using the local equations. There is a limited freedom in the choice of $H(r_{\text{out}})$, which reflects physical uncertainties in the behavior of the disk outside our boundary r_{out} : how far the disk extends beyond r_{out} and how much mass and energy it has lost to a wind. These uncertainties, however, have no impact on

the neutrino-cooled disk at $r < r_{\text{ign}}$ as we verify directly by varying the outer boundary condition: the solution we get at $r \lesssim r_{\text{ign}} \ll r_{\text{out}}$ is the same in all cases. Instead of H/r , one may use energy per baryon U/ρ as a free parameter at the outer boundary. In the advective disk, U/ρ is comparable to the virial specific energy GM/r . In the sample models shown below we specify $U/\rho = GM/r$ at $r = r_{\text{out}}$.

The set of disk equations is a complicated mixture of differential and algebraic equations, which involve integrals of the Fermi-Dirac distribution. We solve these equations on a logarithmic grid r_i ($i = 0..N$), starting at $r_0 = r_{\text{out}}$ and moving inward. At each step, we need to find the parameters of the disk at $r = r_i$ using the known parameters at $r_{i-1} > r_i$ from the previous step.

The state of matter at any radius is described by Y_e and two independent thermodynamic quantities, which we choose to be $\theta = kT/m_e c^2$ and $\eta_e = \mu_e/kT$ (because they enter as parameters in the integrals of Fermi-Dirac distribution). Density ρ , pressure P , and energy density U are expressed in terms of θ , η_e , and Y_e as explained in § 2.3. For example, the expression for ρ is given by the charge neutrality equation (19). The computational problem now reduces to finding θ , η_e , and Y_e at radius r_i given the known parameters at r_{i-1} .

$Y_e(r_i)$ is easily found using the differential equation (9) since $Y_e(r_{i-1})$ is known from the previous step. The main difficulty is in the calculation of $\theta(r_i)$ and $\eta_e(r_i)$. As two independent equations for θ and η_e we choose hydrostatic balance (6) and energy equation (4). The scale-height H that appears in both equations may be expressed in terms of ρ using equations (1), (3), and (6),

$$\left(\frac{H}{r}\right)^3 = \frac{S}{\alpha} \frac{\dot{M}}{4\pi r^2 \rho} \left(\frac{r}{GMJ}\right)^{1/2}. \quad (38)$$

Then the hydrostatic equation becomes

$$P = \left(\frac{S}{\alpha} \frac{GM\dot{M}J}{4\pi r^3}\right)^{2/3} \rho^{1/3}, \quad (39)$$

where $r = r_i$. Both P and ρ are known functions of θ and η_e , which are evaluated numerically. This gives one equation for θ and η_e .

The second (energy) equation is differential and must be discretized,

$$F^+ - F^- = u^r \left[\frac{U_i H_i - U_{i-1} H_{i-1}}{r_i - r_{i-1}} - \frac{(U + P)}{\rho} \frac{(\rho_i H_i - \rho_{i-1} H_{i-1})}{r_i - r_{i-1}} \right]. \quad (40)$$

All quantities taken at point r_{i-1} are known and all quantities taken at r_i are functions of θ and η_e . This gives the second equation.

We find θ and η_e that satisfy both equations (38) and (40) numerically, using a direct search in the (θ, η_e) plane. Once θ and η_e are found at r_i , we calculate all parameters of the disk at this radius and move on to the next step r_{i+1} .

4. RESULTS

4.1. Sample Models

Figures 1-8 show examples of the disk structure for accretion rate $0.2M_\odot \text{ s}^{-1}$ and three different values of viscosity parameter $\alpha = 0.1, 0.03, \text{ and } 0.01$. For comparison two cases are shown: $a = 0$ (Schwarzschild) and $a = 0.95$ (Kerr). The black hole mass $M = 3M_\odot$ is assumed in all models.

First, we note significant differences between models with high $\alpha = 0.1$ and low $\alpha = 0.01$. Disks with low α accrete slower and have higher density. This has the following implications: (1) the region of neutrino emission in low- α disks extends to larger radii $r \sim 200r_g$, (2) electron degeneracy $\eta_e = \mu_e/kT$ is higher, and (3) Y_e is lower.

Electron degeneracy η_e is an important physical parameter that affects Y_e , pressure, and neutrino cooling. In the outer advective region, η_e is decreasing as the heated fluid approaches the black hole until it reaches radii of a few hundred r_g where nuclear cooling F_{nuc} becomes significant. When only $\sim 10\%$ of α -particles are disintegrated (see Fig. 5), an energy $X_f \times 7.1 \text{ MeV} \approx 0.7 \text{ MeV}$ is consumed per nucleon, which is comparable to the available heat stored in the flow at these radii. Then η_e begins to grow.

The evolution of η_e around $100r_g$ is shaped by the competition of a few effects that are sensitive to α . In low- α disks, neutrino emission becomes significant at $r \sim 200r_g$, which implies additional cooling (besides F_{nuc}) and the drop of Y_e from 0.5 toward a low equilibrium value. The coupled evolution of Y_e , η_e , and neutrino emissivity reaches β -equilibrium at $r \sim 50r_g$. In high- α disks, neutrino emission is less efficient at $r \sim 100r_g$ and the drop of Y_e occurs at smaller r , which leads to a different evolution of degeneracy η_e with radius. In all cases, however, β -equilibrium is established with a low Y_e as soon as neutrino emission becomes significant in the energy balance of the disk.

The nuclear cooling becomes negligible where 90% of α -particles disappear (Fig. 5). In the $\alpha = 0.1$ model, the neutrino cooling is still weak at this radius and the accreting fluid is quickly heated by F^+ . This recovery of disk heating leads to the knee in the profile of H/r at $r \approx 40r_g$ (Fig. 6). Then the growth of T above 1 MeV ignites strong neutrino emission that carries away the generated heat and produces the spike of $F_\nu(r)$ between $10r_g$ and $20r_g$,

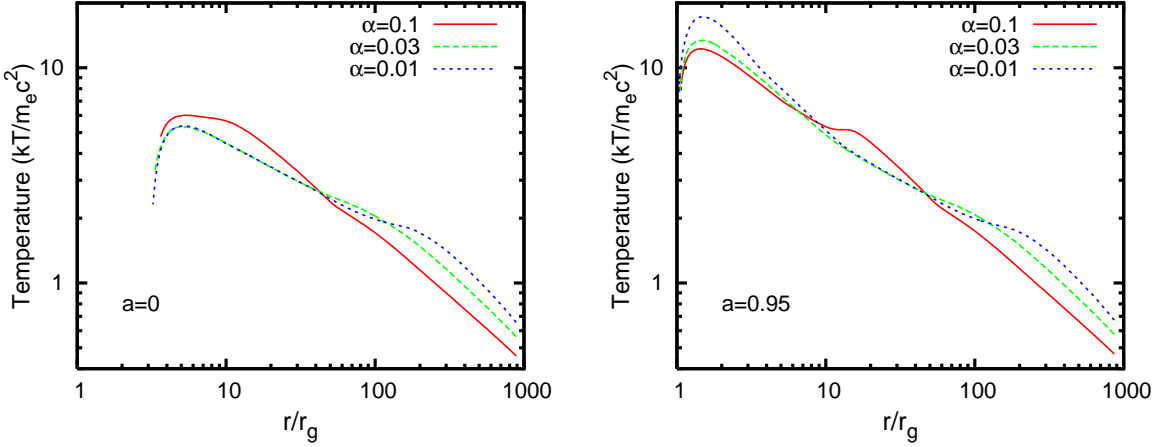


Fig. 1.— Temperature of the accretion disk with $\dot{M} = 0.2M_{\odot} \text{ s}^{-1}$ around a black hole with mass $M = 3M_{\odot}$. Three disk models are shown with different viscosity parameters $\alpha = 0.1$, 0.03, and 0.01. *Left panel*: Schwarzschild black hole ($a = 0$). *Right panel*: Kerr black hole ($a = 0.95$). Radius is shown in units of $r_g = 2GM/c^2$, and temperature in units of $m_e c^2 = 0.511 \text{ MeV}$.

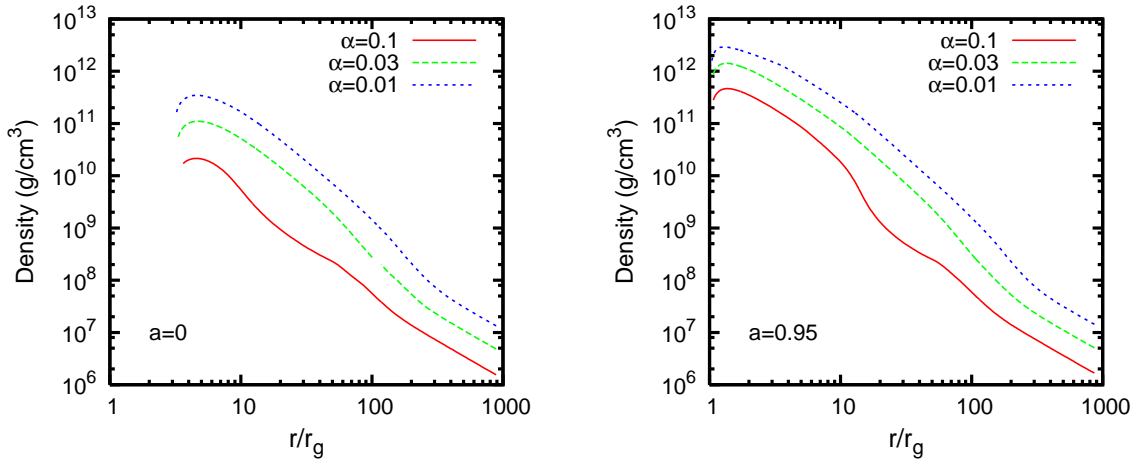


Fig. 2.— Density $\rho(r)$ for the same disk models as in Fig. 1.

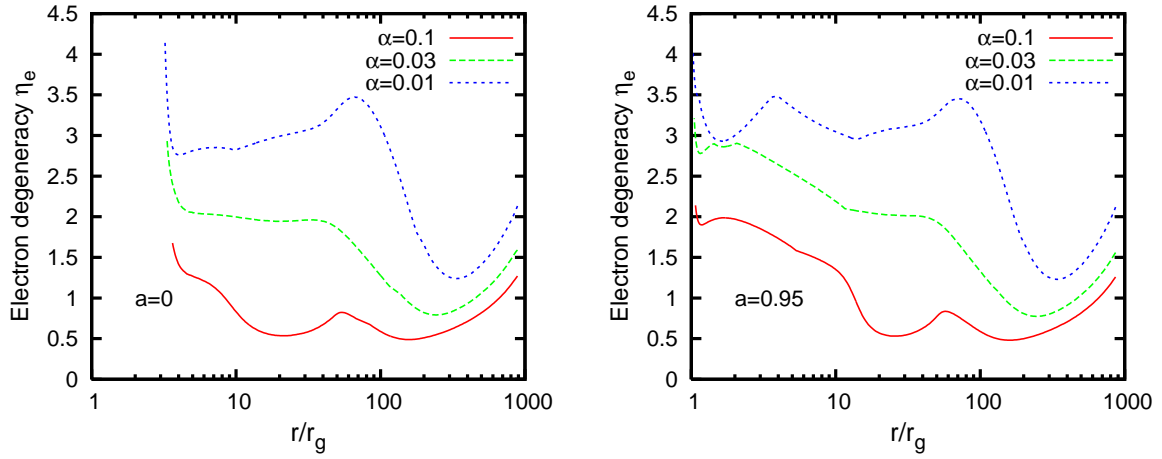


Fig. 3.— Degeneracy parameter $\eta_e(r)$ for the same disk models as in Fig. 1.

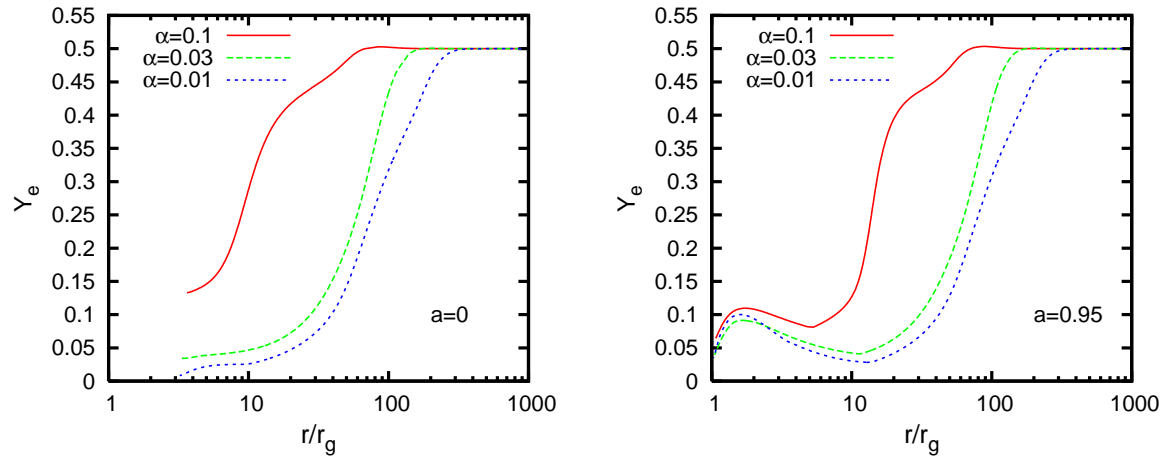


Fig. 4.— $Y_e(r)$ for the same disk models as in Fig. 1.

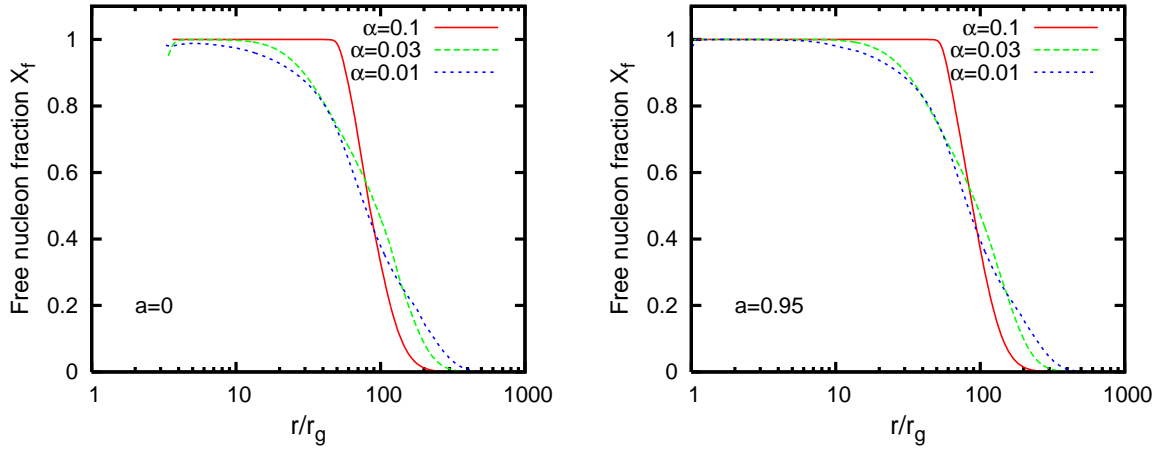


Fig. 5.— Mass fraction of free nucleons $X_f(r)$ for the same disk models as in Fig. 1.

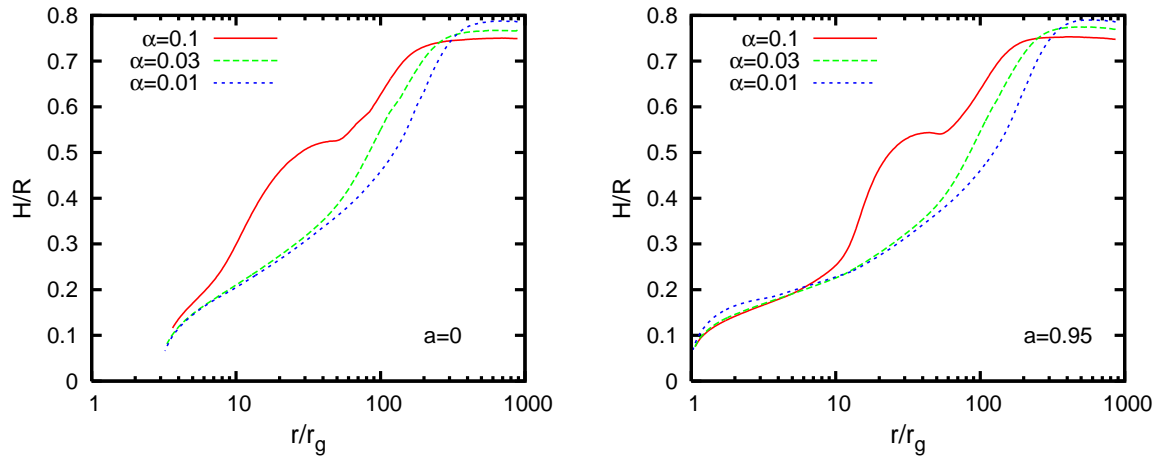


Fig. 6.— Scale-height of the disk $H(r)/r$ for the same disk models as in Fig. 1.

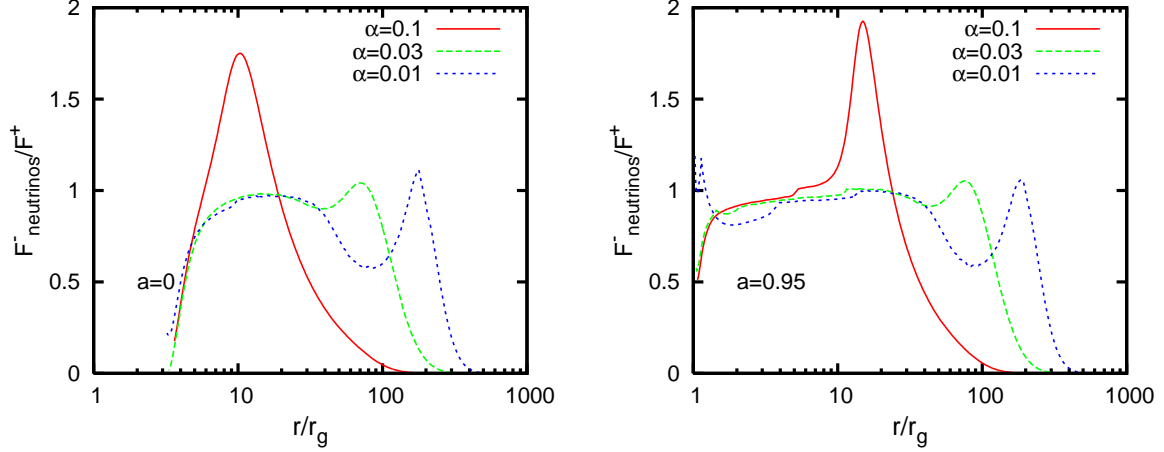


Fig. 7.— Ratio of neutrino flux $F_\nu + F_{\bar{\nu}}$ to the heating rate F^+ for the same disk models as in Fig. 1.

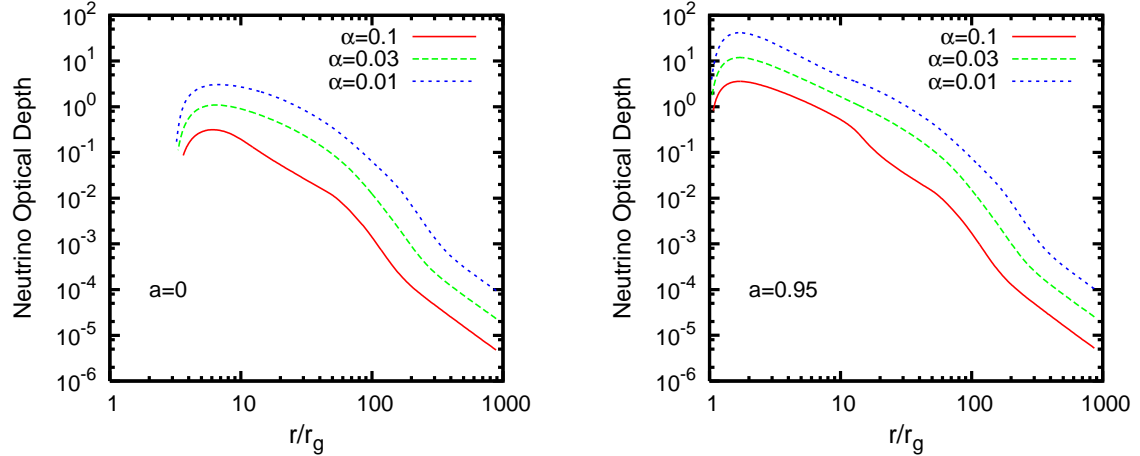


Fig. 8.— Optical depth seen by neutrinos $\tau_\nu(r)$ for the same disk models as in Fig. 1.

overshooting F^+ by a factor of 2 (Fig. 7). This overshooting effect does not happen in the low- α disks because they are cooled more efficiently around $100r_g$.

The Kerr disk models with $a = 0.95$ extend to a small radius $r_{\text{ms}} \approx r_g$ and have an extended neutrino-cooled region where $F^+ \approx F^- \approx F_\nu + F_{\bar{\nu}}$, i.e. the approximate local balance between heating and cooling is established. This balance requires smaller scale-height H/r at smaller radii. As a result, H/r is reduced below 0.2. Significant differences between Schwarzschild and Kerr cases are observed in the inner region $r < 10r_g$ where most of accretion energy is released. The Kerr disk becomes opaque to neutrinos, and the value of Y_e converges to $Y_e \sim 0.1$ for all three viscosity parameters $\alpha = 0.1, 0.03$, and 0.01 .

Figure 9 shows the contributions of P_b , P_γ , $P_e = P_{e-} + P_{e+}$, and P_ν to the total pressure P for two models of Kerr disk. One can see that the baryon pressure P_b dominates in the neutrino-cooled region. This is a general property of all neutrino-cooled disks, which corresponds to their mild degeneracy $\eta_e \sim 1 - 3$. In the limit of strong electron degeneracy, P_e would be dominant. In the limit of low degeneracy, $P_\gamma \sim P_e$ would be dominant. Only at mild degeneracy P_γ and P_e are small compared with P_b . The dominance of P_b is thus a special feature of ν -cooled disks that is related to their self-regulation toward the mild degeneracy and low $Y_e \sim 0.1$.

4.2. Survey of Models

A schematic picture of accretion disk is shown in Figure 10. The disk has 5 characteristic radii:

1. — Radius r_α where 50% of α -particles are decomposed into free nucleons. The destruction of α -particles consumes 7 MeV per nucleon, which makes the disk thinner.
2. — "Ignition" radius r_{ign} where neutrino emission switches on. At this point, the mean electron energy becomes comparable to $(m_n - m_p)c^2$, enabling the capture reaction $e^- + p \rightarrow n + \nu$. Then neutrino cooling becomes significant, further reducing the disk thickness H/r . We choose the condition $F_\nu + F_{\bar{\nu}} = F^+/2$ as a formal definition of r_{ign} .
3. — Radius r_ν where the disk becomes opaque for neutrinos and they relax to a thermal distribution. Note that the disk is still almost transparent for anti-neutrinos at this radius.
4. — Radius $r_{\bar{\nu}}$ where the disk becomes opaque for anti-neutrinos, so that both ν and $\bar{\nu}$ are now in thermal equilibrium with the matter. The disk is still cooled efficiently at this radius since ν and $\bar{\nu}$ diffuse and escape the flow faster than it accretes into the black hole.

5. — Radius r_{tr} where the timescale of neutrino diffusion out of the disk, $t_{\text{diff}} = (H/c)\tau_\nu$ becomes longer than the accretion timescale, and neutrinos get trapped and advected into the black hole. The transition radius r_{tr} is formally defined where $F_\nu + F_{\bar{\nu}}$ drops below $F^+/2$.

In addition, there is a radius beyond which the steady-disk model is inconsistent because of gravitational instability (e.g. Paczyński 1978). We estimate this boundary from the condition

$$Q = \frac{c_s \Omega}{2\pi G H \rho} \approx 1. \quad (41)$$

The unstable region is where $Q < 1$. Besides the gravitational instability, the disk mass in this region becomes comparable to that of the black hole, and the gravitational potential is not described by the Kerr metric.

We ran a series of models with various \dot{M} , for two values of the spin parameter $a = 0$ and $a = 0.95$. For each model, we found the five characteristic radii and the region of gravitational instability. The results are summarized in Figures 11 and 12. Contour plots of temperature T , density ρ , electron fraction Y_e , and efficiency of local cooling $(F_\nu + F_{\bar{\nu}})/F^+$ are shown in Figures 13-16.

As one can see from Figures 11 and 12, the radius of 50% disintegration of α -particles exists at all \dot{M} of the sequence ($\dot{M} \gtrsim 10^{-3} M_\odot \text{ s}^{-1}$) and weakly depends on \dot{M} . In most models it is between 40 and $100r_g$.

The ignition radius r_{ign} exists if $\dot{M} > \dot{M}_{\text{ign}}$ which depends on α and a . Disks with $\dot{M} < \dot{M}_{\text{ign}}$ remain advective all the way to the black hole. For example, for the Kerr disk with $a = 0.95$ and $\alpha = 0.1$, $\dot{M}_{\text{ign}} \approx 0.02 M_\odot \text{ s}^{-1}$. By contrast, for the Schwarzschild disk with the same $\alpha = 0.1$, $\dot{M}_{\text{ign}} \approx 0.07 M_\odot \text{ s}^{-1}$. One can see in Figures 11 and 12 that the ignition radius first appears in the inner region when $\dot{M} = \dot{M}_{\text{ign}}$. As \dot{M} increases r_{ign} moves to $\sim 100r_g$.

The radii of transparency, r_ν and $r_{\bar{\nu}}$, scale with \dot{M} approximately as $\dot{M}^{3/2}$, and $r_\nu \approx 2r_{\bar{\nu}}$. Transparency of the disk for neutrinos also depends on the black-hole spin. The disk becomes opaque if $\dot{M} > \dot{M}_{\text{opaque}} \approx 0.1 M_\odot \text{ s}^{-1}$ in the Kerr case ($a = 0.95$) and if $\dot{M} > \dot{M}_{\text{opaque}} \approx 1 M_\odot \text{ s}^{-1}$ in the Schwarzschild case.

Significant trapping of neutrinos occurs in the inner region of the Kerr disk if $\dot{M} > \dot{M}_{\text{trap}}$ which also depends on α and a . For example, for $\alpha = 0.1$, $\dot{M}_{\text{trap}} \approx 2 M_\odot \text{ s}^{-1}$ if $a = 0.95$ and $\dot{M}_{\text{trap}} \approx 10 M_\odot \text{ s}^{-1}$ if $a = 0$. The trapping radius r_{tr} grows linearly with \dot{M} .

It is worth emphasizing that all three characteristic accretion rates, \dot{M}_{ign} , \dot{M}_{opaque} , and \dot{M}_{trap} are lower for disks with smaller viscosity parameter α . The low- α disks are denser and have significantly larger r_ν and r_{tr} . For example, the radius of opaqueness r_ν in the models

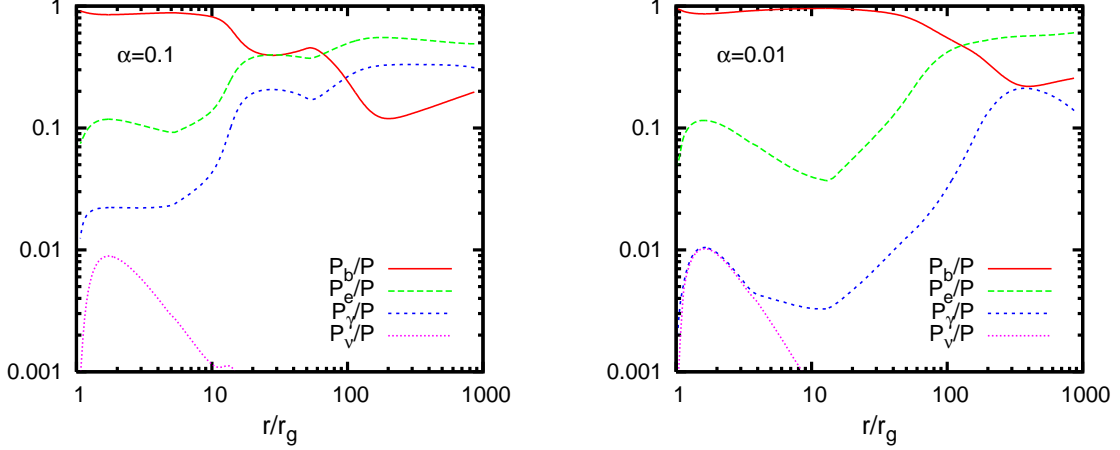


Fig. 9.— Contributions to total pressure P from baryons, P_b , electrons and positrons $P_e = P_{e-} + P_{e+}$, radiation P_γ , and neutrinos $P_\nu + P_{\bar{\nu}}$ for the Kerr accretion disk ($a = 0.95$) with $\dot{M} = 0.2M_\odot \text{ s}^{-1}$. *Left panel*: model with viscosity parameter $\alpha = 0.1$. *Right panel*: model with $\alpha = 0.01$.

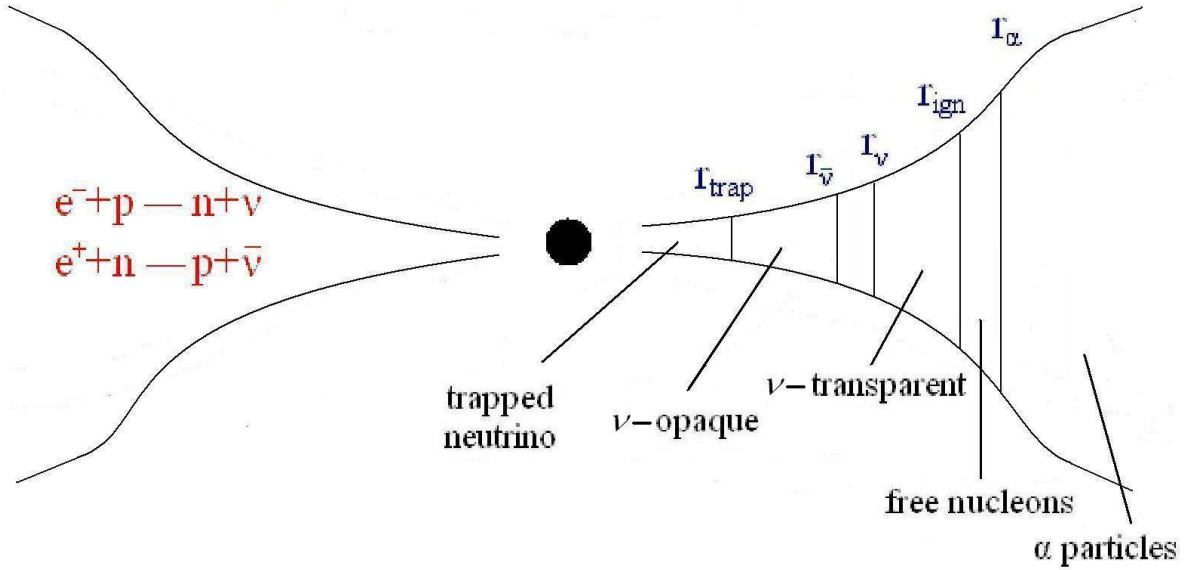


Fig. 10.— Schematic picture of the disk with characteristic radii indicated.

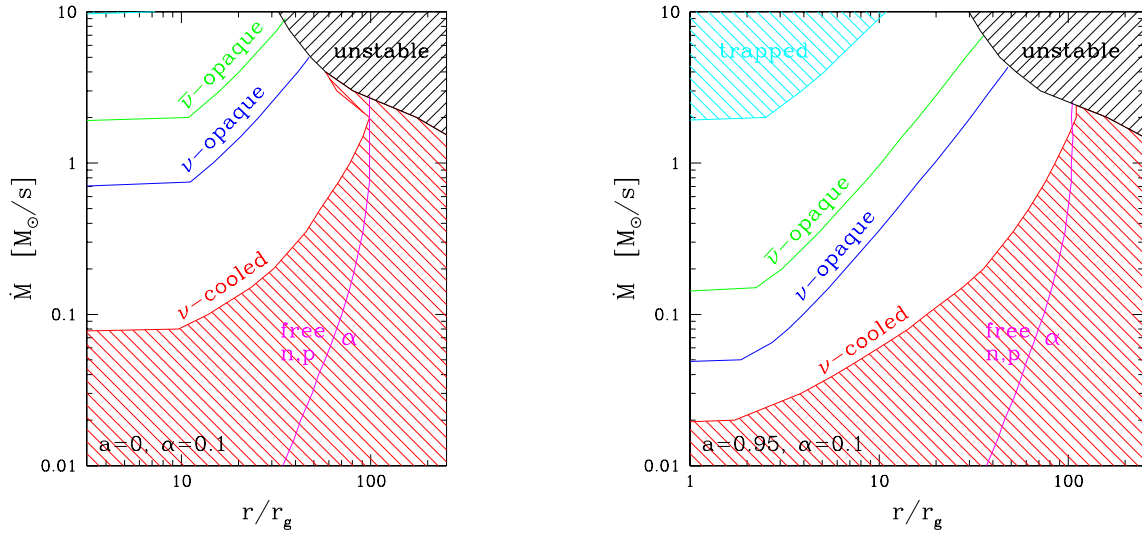


Fig. 11.— Boundaries of different regions on the $r\dot{M}$ plane for disks around a black hole of mass $M = 3M_\odot$ and spin parameter $a = 0$ (left) and 0.95 (right). Viscosity parameter $\alpha = 0.1$ is assumed. Neutrino cooling is small in the shadowed region below the “ ν -cooled” curve and above the “trapped” curve. The shadowed region marked “unstable” is excluded: the steady model is inconsistent in this region because of the gravitational instability. The disk extends down to the marginally stable orbit of radius $r_{\text{ms}} = 3r_g$ for $a = 0$ and $r_{\text{ms}} \approx r_g$ for $a = 0.95$, where $r_g = 2GM/c^2$.

with $\alpha = 0.01$ is almost one order of magnitude larger than in $\alpha = 0.1$ models.

The dependence of \dot{M}_{ign} , \dot{M}_{opaque} , and \dot{M}_{trap} on α is well approximated by a power law (see Fig. 13),

$$\dot{M}_{\text{ign}} = K_{\text{ign}} \left(\frac{\alpha}{0.1} \right)^{5/3}, \quad \dot{M}_{\text{opaque}} = K_{\text{opaque}} \left(\frac{\alpha}{0.1} \right), \quad \dot{M}_{\text{trap}} = K_{\text{trap}} \left(\frac{\alpha}{0.1} \right)^{1/3}. \quad (42)$$

where the normalization factors K depend on the black hole spin a . For $a = 0$, we find $K_{\text{ign}} = 0.071 M_{\odot} \text{ s}^{-1}$, $K_{\text{opaque}} = 0.7 M_{\odot} \text{ s}^{-1}$, and $K_{\text{trap}} = 9.3 M_{\odot} \text{ s}^{-1}$. For $a = 0.95$, we find $K_{\text{ign}} = 0.021 M_{\odot} \text{ s}^{-1}$, $K_{\text{opaque}} = 0.06 M_{\odot} \text{ s}^{-1}$, and $K_{\text{trap}} = 1.8 M_{\odot} \text{ s}^{-1}$.

The maximum radiative efficiency of the disk, $L_{\nu}/\dot{M}c^2$, is determined by the binding energy at the last stable orbit r_{ms} . It equals 0.057 for $a = 0$ and 0.19 for $a = 0.95$. The real efficiency is somewhat smaller because part of the released energy remains stored in the disk and advected into the black hole. The efficiency is shown as a function of \dot{M} in Figure 18.

5. CONCLUSIONS

This paper presents the model of neutrino-cooled accretion disks around rotating black holes that calculates self-consistently nuclear composition, neutrino emission, and fluid dynamics in the Kerr metric. The model is one-dimensional in the sense that all parameters of the disk are integrated/averaged in the vertical direction and depend on r only, and the standard α -prescription is used for viscosity. The model also assumes a steady state, which is applicable only to radii where accretion timescale is shorter than the timescale of variation of \dot{M} in the problem. The main advance of our work compared with PWF is the calculation of electron degeneracy and nuclear composition of the accreting matter; both dramatically affect the disk and its neutrino emission.

The disk has a clear structure with five characteristic radii r_{α} , r_{ign} , r_{ν} , $r_{\bar{\nu}}$, and r_{tr} . Radial advection of lepton number Y_e and viscously dissipated heat is important outside the ignition radius r_{ign} . Most of the viscous heat is lost to neutrino emission at $r < r_{\text{ign}}$.

The neutrino-cooled disk forms at accretion rates $\dot{M} > \dot{M}_{\text{ign}}$ which depends on the black-hole spin a and the viscosity parameter α (see Fig. 17 and eq. 42). General properties of the ν -cooled disk are as follows.

1. — The disk is relatively thin, $H/r \sim 0.1 - 0.3$, especially in the inner region where most of accretion energy is released. The outer advective region $r \gtrsim 100r_g$ is also significantly cooled by the gradual disintegration of α -particles, and its thickness is reduced.
2. — The ν -cooled disk is nearly in β -equilibrium, in agreement with analytical estimates

(Beloborodov 2003a). In particular, the relation between ρ , T , and Y_e calculated under the equilibrium assumption (Fig. 1 and 2 in Beloborodov 2003a) applies with a high accuracy.

3. — Degeneracy of electrons in the disk significantly suppresses the positron density n_{e^+} . However, the strong degeneracy limit is not applicable — the disk regulates itself to a mildly degenerate state. The reason of this regulation is the negative feedback of degeneracy on the cooling rate: higher degeneracy $\mu_e/kT \rightarrow$ fewer electrons (lower Y_e) and positrons ($n_{e^+}/n_{e^-} \sim e^{-\mu_e/kT}$) \rightarrow weaker neutrino emission \rightarrow lower cooling rate \rightarrow higher temperature \rightarrow lower degeneracy.

4. — Pressure in ν -cooled disks is dominated by baryons, $P \approx P_b = (\rho/m_p)kT$, most of which are neutrons.

5. — All ν -cooled disks are very neutron rich in the inner region, with $Y_e \sim 0.1$ or lower.

The high neutron richness has important implications for the global picture of GRB explosion (e.g. Derishev, Kocharovsky, & Kocharovsky 1999; Beloborodov 2003a,b; Rossi, Beloborodov, & Rees 2006). When the neutron-rich material is ejected in a relativistic jet, it develops a large Lorentz factor, and the neutrons gradually decay on scales up to 10^{17} cm where the GRB blast wave is observed.

The disks around rapidly rotating black holes are markedly different from disks around Schwarzschild black holes. They extend much closer to the center and reach higher temperatures and densities. For example, we found that the disk with $\alpha = 0.1$ around a Kerr black hole with $a = 0.95$ becomes opaque for neutrinos at $\dot{M}_{\text{opaque}} \sim 0.07M_{\odot} \text{ s}^{-1}$, which is 10 times lower than the corresponding \dot{M}_{opaque} for a Schwarzschild black hole. Besides, Kerr disks produce much higher neutrino fluxes in the inner region, with a higher mean energy per neutrino. The annihilation reaction $\nu + \bar{\nu} \rightarrow e^+ + e^-$ deposits energy above the disk and can drive a powerful outflow that will be investigated elsewhere.

This work was supported by NASA grant NAG5-13382.

Appendix A: Radial Velocity in a Relativistic Disk

Conservation of energy and angular momentum is expressed by the equations (see Beloborodov, Abramowicz, & Novikov 1997)

$$\frac{d}{dr} \left[\mu \left(\frac{\dot{M}u_t}{2\pi} + 2\nu\Sigma r\sigma_t^r \right) \right] = \frac{F^-}{c^2}ru_t, \quad (43)$$

$$\frac{d}{dr} \left[\mu \left(\frac{\dot{M} u_\phi}{2\pi} + 2\nu \Sigma r \sigma_\phi^r \right) \right] = \frac{F^-}{c^2} r u_\phi, \quad (44)$$

where

$$\sigma_\phi^r = \frac{1}{2} g^{rr} g_{\phi\phi} \sqrt{-g^{tt}} \gamma^3 \frac{d\Omega}{dr} \quad (45)$$

is the shear and $\mu = (U + P)/\rho c^2$ is the relativistic enthalpy per unit rest mass ($\mu \approx 1$ in the neutrino-cooled disk); $\gamma = u^t/\sqrt{-g^{tt}}$ and $\Omega = u^\phi/u^t$ are taken for the Keplerian circular motion (eq. 2). From equations (43) and (44) one can derive (see also Page & Thorne 1974)

$$\begin{aligned} 2\nu \Sigma r \sigma_\phi^r = T(x) = & -\frac{\dot{M}}{2\pi} \frac{GM}{c} \frac{x^3 + a}{(x^3 - 3x + 2a)^{1/2} x^{3/2}} \left[(x - x_0) - \frac{3}{2} a \ln\left(\frac{x}{x_0}\right) \right. \\ & - \frac{3(x_1 - a)^2}{x_1(x_1 - x_2)(x_1 - x_3)} \ln\left(\frac{x - x_1}{x_0 - x_1}\right) - \frac{3(x_2 - a)^2}{x_2(x_2 - x_1)(x_2 - x_3)} \ln\left(\frac{x - x_2}{x_0 - x_2}\right) \\ & \left. - \frac{3(x_3 - a)^2}{x_3(x_3 - x_1)(x_3 - x_2)} \ln\left(\frac{x - x_3}{x_0 - x_3}\right) \right] \end{aligned}$$

where $x = (rc^2/GM)^{1/2}$, x_1, x_2, x_3 are the three roots of equation $x^3 - 3x + 2a = 0$, and x_0 corresponds to the marginally stable orbit r_{ms} where fluid falls freely into the black hole and zero viscous torque is assumed.

The radial velocity u^r may now be expressed as

$$u^r = \frac{\dot{M}}{2\pi r \Sigma} = \frac{\dot{M}}{\pi} \frac{\nu \sigma_\phi^r}{T} \quad (46)$$

where $\sigma_\phi^r(r)$ and $T(r)$ are known functions given by equations (45) and (46). Substituting the α prescription for the kinematic viscosity coefficient, $\nu = (2/3)\alpha c_s H$, one finds

$$u^r = \alpha c_s \left(\frac{H}{r} \right) \frac{2\dot{M}}{3\pi} \frac{r \sigma_\phi^r}{T} = \alpha c_s \left(\frac{H}{r} \right) S^{-1}(r). \quad (47)$$

The numerical factor $S(r) = (3\pi/2)(T/\dot{M}r\sigma_\phi^r)$ varies from zero at the inner radius r_{ms} to unity at $r \gg r_g$.

“Newtonian” approximation that is often used in the literature on accretion disks (including GRB disks) is given by

$$S_N(r) = 1 - \left(\frac{r_{\text{ms}}}{r} \right)^{1/2}.$$

It is derived for the accretion disk in Newtonian space by requiring conservation of angular momentum and imposing zero torque at a specified radius r_{ms} , e.g. $r_{\text{ms}} = 3r_g$ to mimic a Schwarzschild spacetime (Shakura & Sunyaev 1973). The correct function S differs significantly from S_N even for a Schwarzschild black hole: $S \lesssim S_N/2$ in the inner region of the disk.

Appendix B: Cross Sections for Neutrino Interactions

We summarize here the cross sections of neutrino reactions that we use in this paper (see Burrows & Thompson 2002 for a recent review of the reactions). The cross sections are expressed in terms of σ_0 ,

$$\sigma_0 = \frac{4G_F^2(m_e c^2)^2}{\pi(\hbar c)^4} \simeq 1.71 \times 10^{-44} \text{ cm}^2. \quad (48)$$

The neutrino energy is denoted by E and expressed in units of $m_e c^2$.

1. — Neutrino absorption by nucleons:

$$\nu + n \rightarrow e^- + p, \quad \bar{\nu} + p \rightarrow e^+ + n \quad (49)$$

The cross section of ν absorption by neutron is given by (e.g. Bemporad et al. 2002)

$$\sigma_{\nu n}(E_\nu) = \sigma_0 \left(\frac{1 + 3g_A^2}{4} \right) (E_\nu + Q)^2 \sqrt{1 - \frac{1}{(E_\nu + Q)^2}}, \quad (50)$$

where $Q = (m_n - m_p)/m_e = 2.53$, $g_A \simeq -1.26$ is the axial coupling constant, $(1 + 3g_A^2)/4 \simeq 1.44$. This approximation neglects the recoil of neutron, however, it has only a small error $< 1.5\%$ when the neutrino energy is below 80 MeV (Strumia & Vissani 2003). For $\bar{\nu}$ absorption by protons, however, there is a significant correction due to the recoil, and a better approximation should be used. We use the approximation of Strumia & Vissani (2003),

$$\begin{aligned} \sigma_{\bar{\nu} p}(E_{\bar{\nu}}) &= 10^{-43} \kappa^2 (E_{\bar{\nu}} - Q)^2 \sqrt{1 - \frac{1}{\kappa^2(E_{\bar{\nu}} - Q)^2}} \\ &\times (\kappa E_{\bar{\nu}})^{-0.07056 + 0.02018 \ln(\kappa E_{\bar{\nu}}) - 0.001953 \ln^3(\kappa E_{\bar{\nu}})} \text{ cm}^2. \end{aligned}$$

where $\kappa = 0.511$.

2. — Neutrino-baryon elastic scattering. The cross sections of scattering on proton, neutron, and α particles are

$$\sigma_p(E) = \frac{\sigma_0 E^2}{4} \left[4 \sin^4 \theta_W - 2 \sin^2 \theta_W + \frac{1 + 3g_A^2}{4} \right] = 0.30 \sigma_0 E^2, \quad (51)$$

$$\sigma_n(E) = \frac{\sigma_0 E^2}{4} \left(\frac{1 + 3g_A^2}{4} \right) = 0.36 \sigma_0 E^2, \quad (52)$$

$$\sigma_\alpha(E) = 4 \sigma_0 \sin^4 \theta_W E^2 = 0.21 \sigma_0 E^2, \quad (53)$$

where θ_W is the Weinberg angle and $\sin^2 \theta_W = 0.23$.

3. — Neutrino-electron (or neutrino-positron) scattering. The cross section of scattering for ν or $\bar{\nu}$ is given by (Burrows & Thompson 2002),

$$\sigma_e(E) = \frac{3}{8} \sigma_0 \theta E \left(1 + \frac{\eta_e}{4}\right) \left[(C_V + C_A)^2 + \frac{1}{3} (C_V - C_A)^2 \right], \quad (54)$$

where $\theta = kT/(m_e c^2)$ is temperature, $\eta_e = \mu_e/kT$ is the degeneracy parameter, $C_A = +1/2$ for ν and $C_A = -1/2$ for $\bar{\nu}_e$, and $C_V = \frac{1}{2} + 2 \sin^2 \theta_W$ for both ν and $\bar{\nu}$.

4. — Neutrino annihilation: $\nu + \bar{\nu} \rightarrow e^- + e^+$. Considering both the neutral and charged current reactions, the total cross section at high energies $E_\nu, E_{\bar{\nu}} \gg 1$ is given by

$$\sigma_{\nu\bar{\nu}} = K_{\nu\bar{\nu}} \sigma_0 \frac{(\mathbf{P}_\nu \cdot \mathbf{P}_{\bar{\nu}})^2}{E_\nu E_{\bar{\nu}}}, \quad (55)$$

where \mathbf{P}_ν and $\mathbf{P}_{\bar{\nu}}$ are the four-momenta of ν and $\bar{\nu}$ in units of $m_e c$, and $K_{\nu\bar{\nu}} = (1 + 4 \sin^2 \theta_W + 8 \sin^4 \theta_W)/12 = 0.195$ (Goodman et al. 1987; the full expression is found in Dicus 1972). After averaging over target distribution, one gets the average cross section for neutrino and anti-neutrino,

$$\sigma_\nu(E_\nu) = \frac{4}{3} K_{\nu\bar{\nu}} \sigma_0 E_\nu \bar{E}_{\bar{\nu}} \quad (56)$$

$$\sigma_{\bar{\nu}}(E_{\bar{\nu}}) = \frac{4}{3} K_{\nu\bar{\nu}} \sigma_0 E_{\bar{\nu}} \bar{E}_\nu \quad (57)$$

where \bar{E}_ν and $\bar{E}_{\bar{\nu}}$ are the average energies of neutrinos and anti-neutrinos, respectively.

REFERENCES

- Balbus, S. A., & Hawley J. F. 1998, Rev. Mod. Phys., 70, 1
 Beloborodov, A. M. 1998, MNRAS, 297, 739
 Beloborodov, A. M. 1999, ASP Conference Series 161, 295
 Beloborodov, A. M. 2003a, ApJ, 588, 931
 Beloborodov, A. M. 2003b, ApJ, 585, L19
 Beloborodov, A. M., Abramowicz, M. A., & Novikov, I. D. 1997, ApJ, 491, 267
 Bemporad, C., Gratta, G., & Vogel, P. 2002, Rev. Mod. Phys., 74, 297
 Burrows, A., & Thompson, T.A. 2002, astro-ph/0211404
 Dicus, D. A. 1972, Phys. Rev. D, 6, 941

- Derishev, E. V., Kocharovskiy, V. V., & Kocharovskiy, Vl. V. 1999, *ApJ*, 521, 640
- Di Matteo, T., Perna, R., & Narayan, R. 2002, *ApJ*, 579, 706
- Goodman, J., Dar, A., & Nussinov, S. 1987, *ApJ*, 314, L7
- Kohri, K., & Mineshige, S. 2002, *ApJ*, 577, 311
- Kohri, K., Narayan, R. & Piran, T. 2005, *ApJ*, 629, 341
- MacFadyen, A. I., & Woosley, S.E. 1999, *ApJ*, 524, 262
- Meyer, B. S. 1994, *ARA&A*, 32, 153
- Misner, C. W., Thorne, K. S., & Wheeler, J. A. 1973, *Gravitation* (San Francisco: Freeman)
- Narayan, R., Piran, T., & Kumar, P. 2001, *ApJ*, 557, 949
- Narayan, R., & Yi, I. 1994, *ApJ*, L13
- Paczynski, B. 1978, *AcA*, 28, 91
- Page, D. N., & Thorne, K. S. 1974, *ApJ*, 191, 499
- Piran, T. 2004, *Rev. Mod. Phys.*, 76, 1143
- Popham, R., Woosley, S. E., & Fryer, C. 1999, *ApJ*, 518, 356 (PWF)
- Pruet, J., Woosley, S. E., & Hoffman, R. D. 2003, 586, 1254
- Rossi, E., Beloborodov, A. M., & Rees, M. J. 2006, *MNRAS*, in press (astro-ph/0512495)
- Ruffert, M., Janka, H.-T., Takahashi, K., & Schaefer, G. 1997, *A&A*, 319, 122
- Sawyer, R. F. 2003, *Phys. Rev. D*, 68, 063001
- Shakura, N. I., & Sunyaev, R. A. 1973, *A&A*, 24, 337
- Shapiro, S. L., & Teukolsky, S. L. 1983, *Black Holes, White Dwarfs, and Neutron Stars* (New York: Wiley)
- Strumia, A., & Vissani, F. 2003, *Phys. Lett. B*, 564, 42
- Thompson, T. A., Burrows, A., Horvath 2000, *Phys.*, C62, 35802
- Woosley, S. E. 1993, *ApJ*, 405, 273

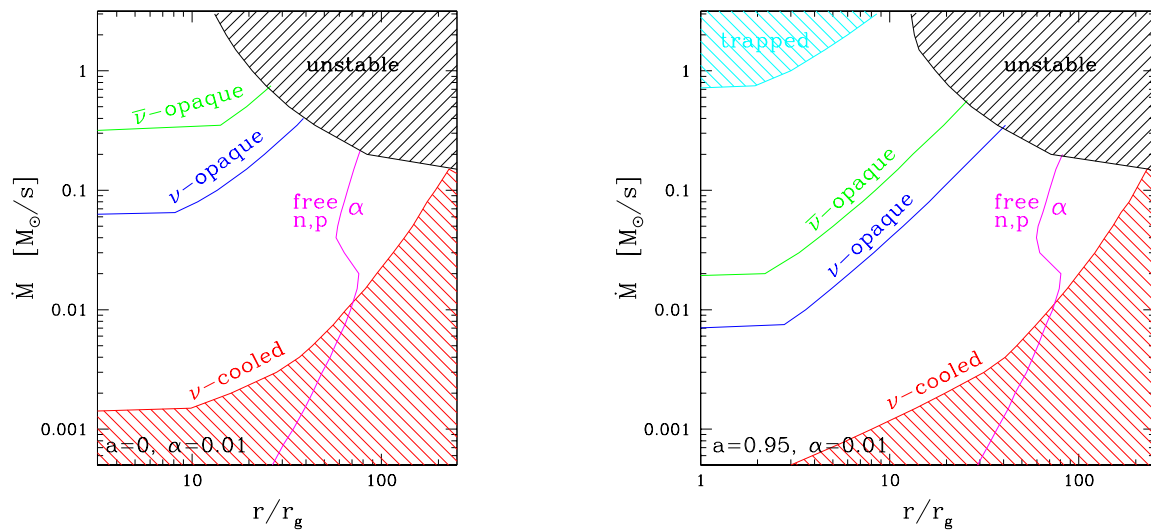


Fig. 12.— Same as Fig. 11 but for $\alpha = 0.01$.

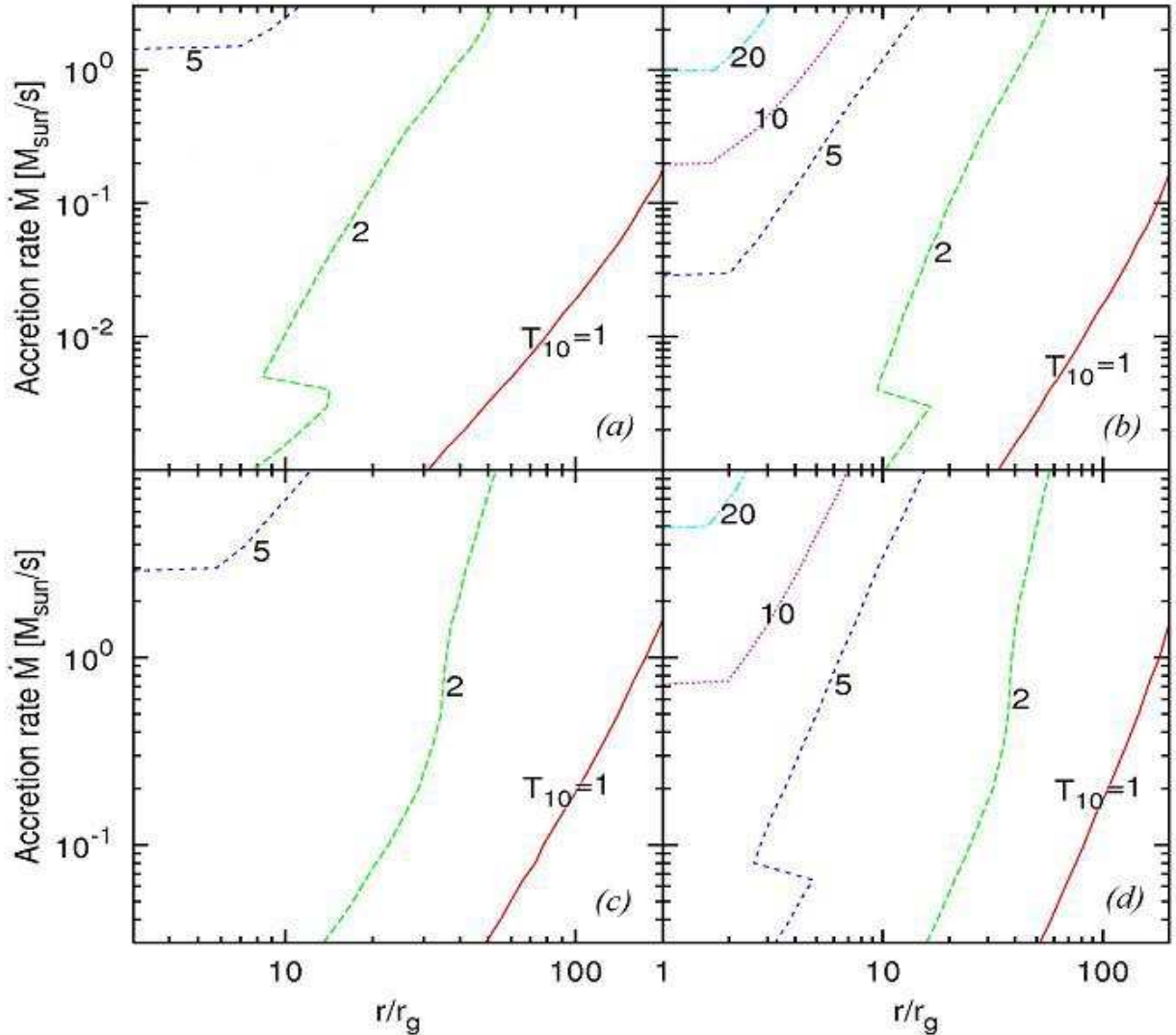


Fig. 13.— Contours of temperature T (in units of 10^{10} K) on the $r - \dot{M}$ plane. (a) $\alpha = 0.01$ and $a = 0$. (b) $\alpha = 0.01$ and $a = 0.95$. (c) $\alpha = 0.1$ and $a = 0$. (d) $\alpha = 0.1$ and $a = 0.95$.

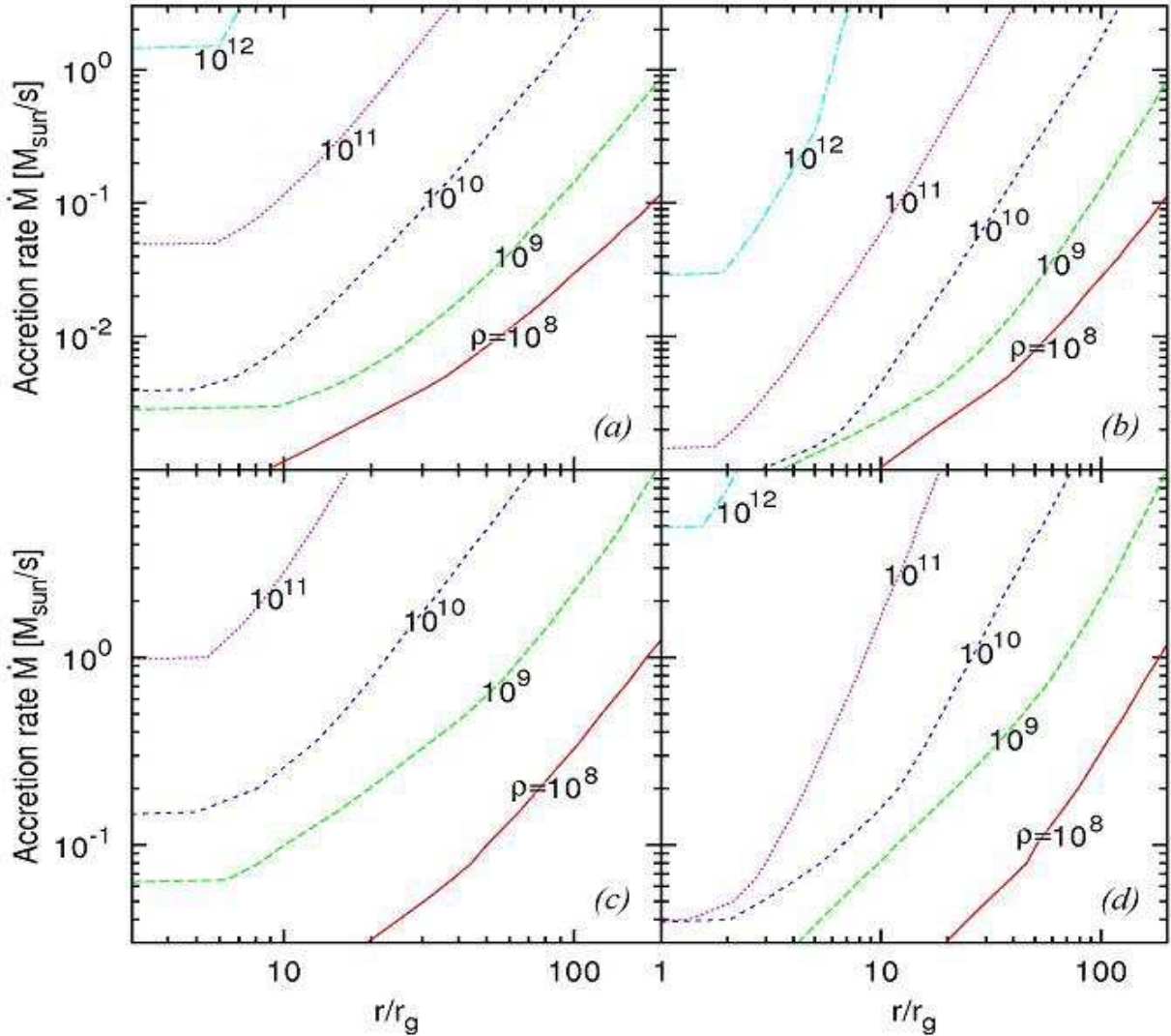


Fig. 14.— Contours of density ρ (in units of g cm^{-3}) on the $r - \dot{M}$ plane. (a) $\alpha = 0.01$ and $a = 0$. (b) $\alpha = 0.01$ and $a = 0.95$. (c) $\alpha = 0.1$ and $a = 0$. (d) $\alpha = 0.1$ and $a = 0.95$.

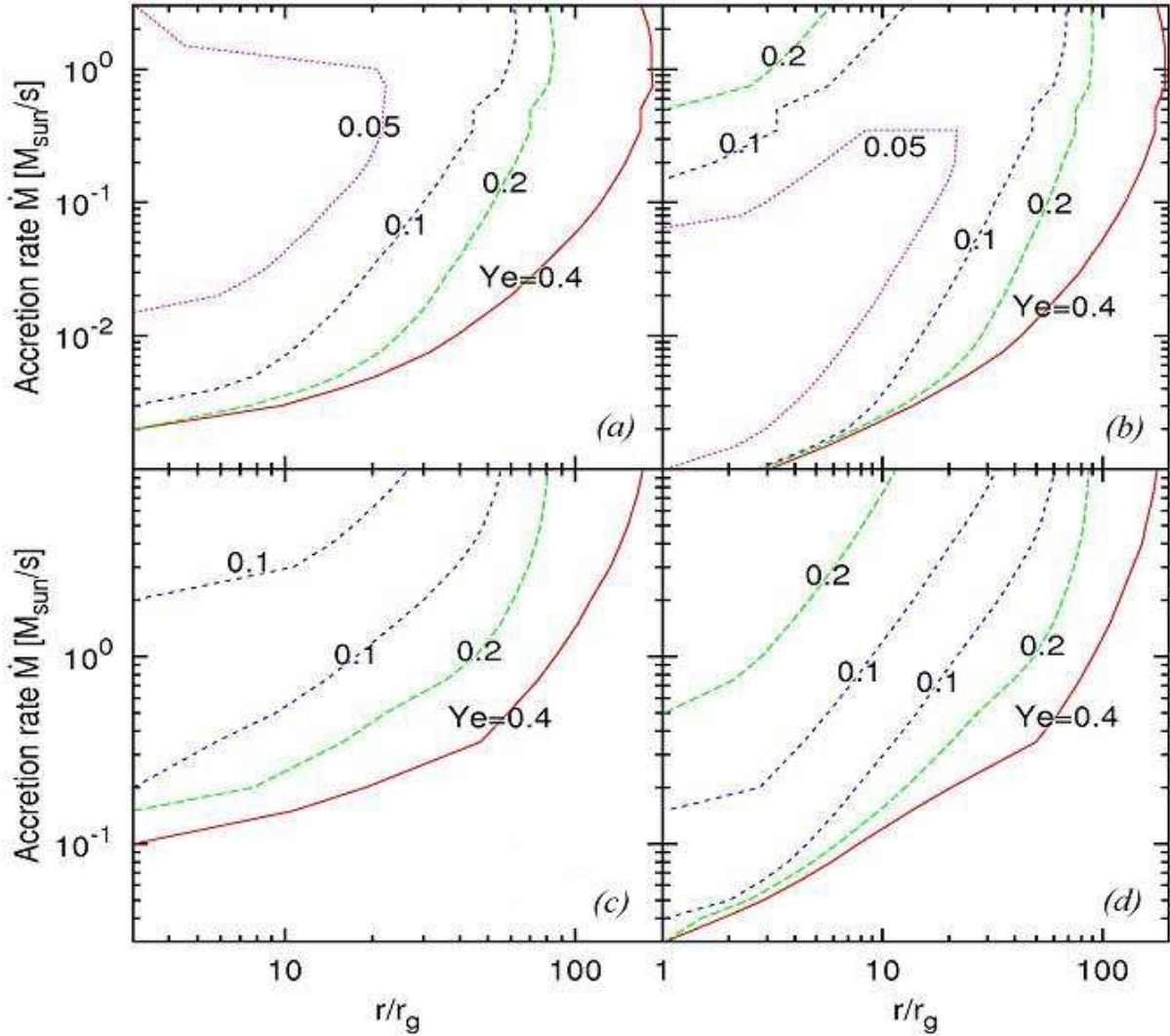


Fig. 15.— Contours of Y_e on the $r - \dot{M}$ plane. (a) $\alpha = 0.01$ and $a = 0$. (b) $\alpha = 0.01$ and $a = 0.95$. (c) $\alpha = 0.1$ and $a = 0$. (d) $\alpha = 0.1$ and $a = 0.95$.

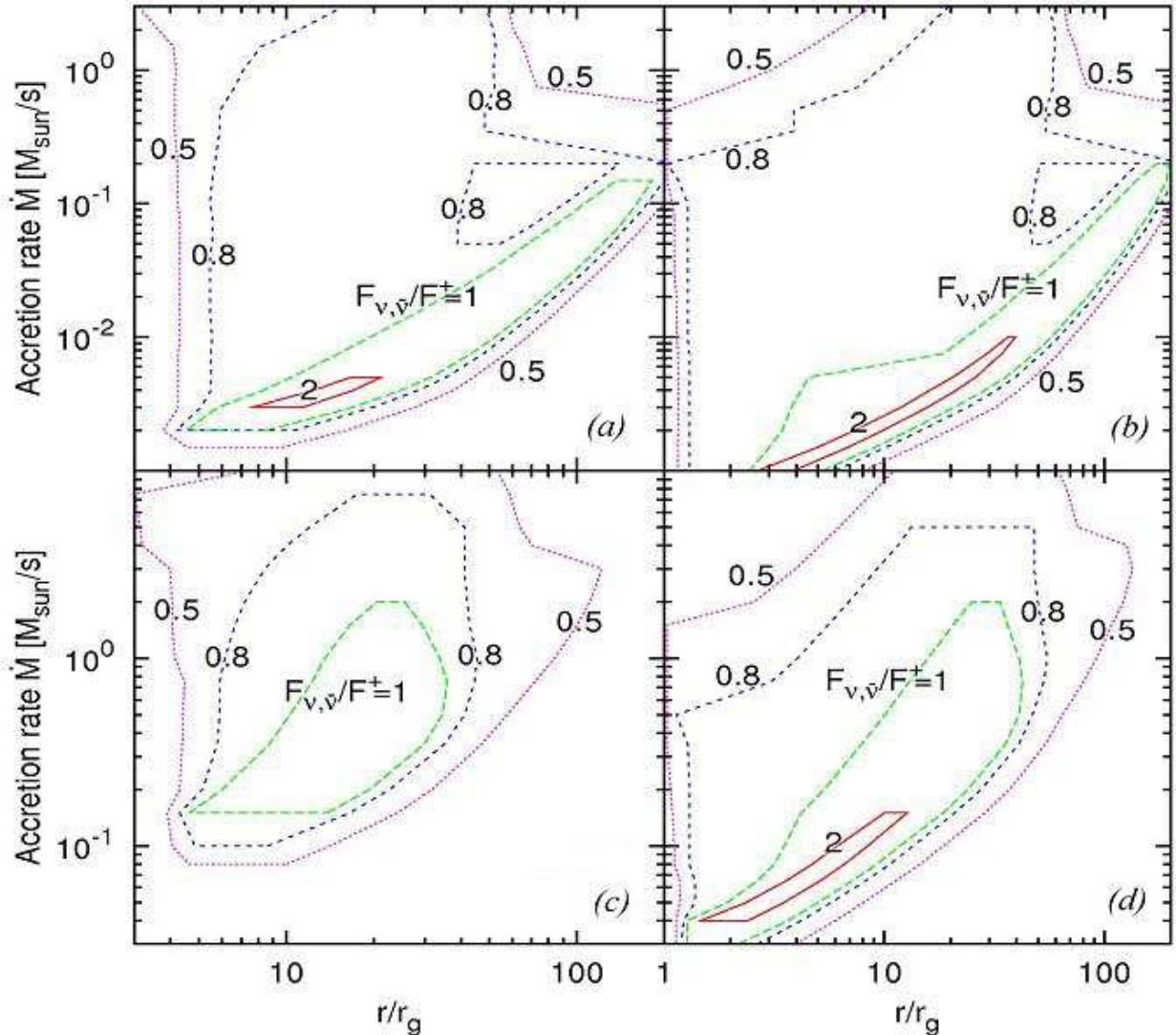


Fig. 16.— Contours of local cooling efficiency $(F_\nu + F_{\bar{\nu}})/F^+$ on the $r - \dot{M}$ plane. (a) $\alpha = 0.01$ and $a = 0$. (b) $\alpha = 0.01$ and $a = 0.95$. (c) $\alpha = 0.1$ and $a = 0$. (d) $\alpha = 0.1$ and $a = 0.95$.

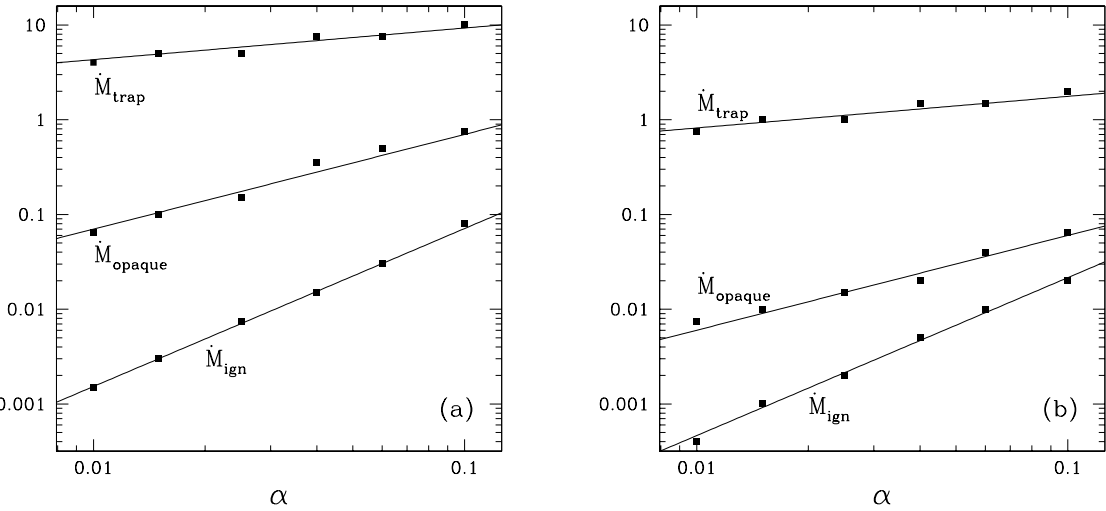


Fig. 17.— Characteristic accretion rates \dot{M}_{ign} , \dot{M}_{opaque} , and \dot{M}_{trap} . The lines show the power-law approximation (eq. 42). (a) Schwarzschild disk ($a = 0$). (b) Kerr disk ($a = 0.95$).

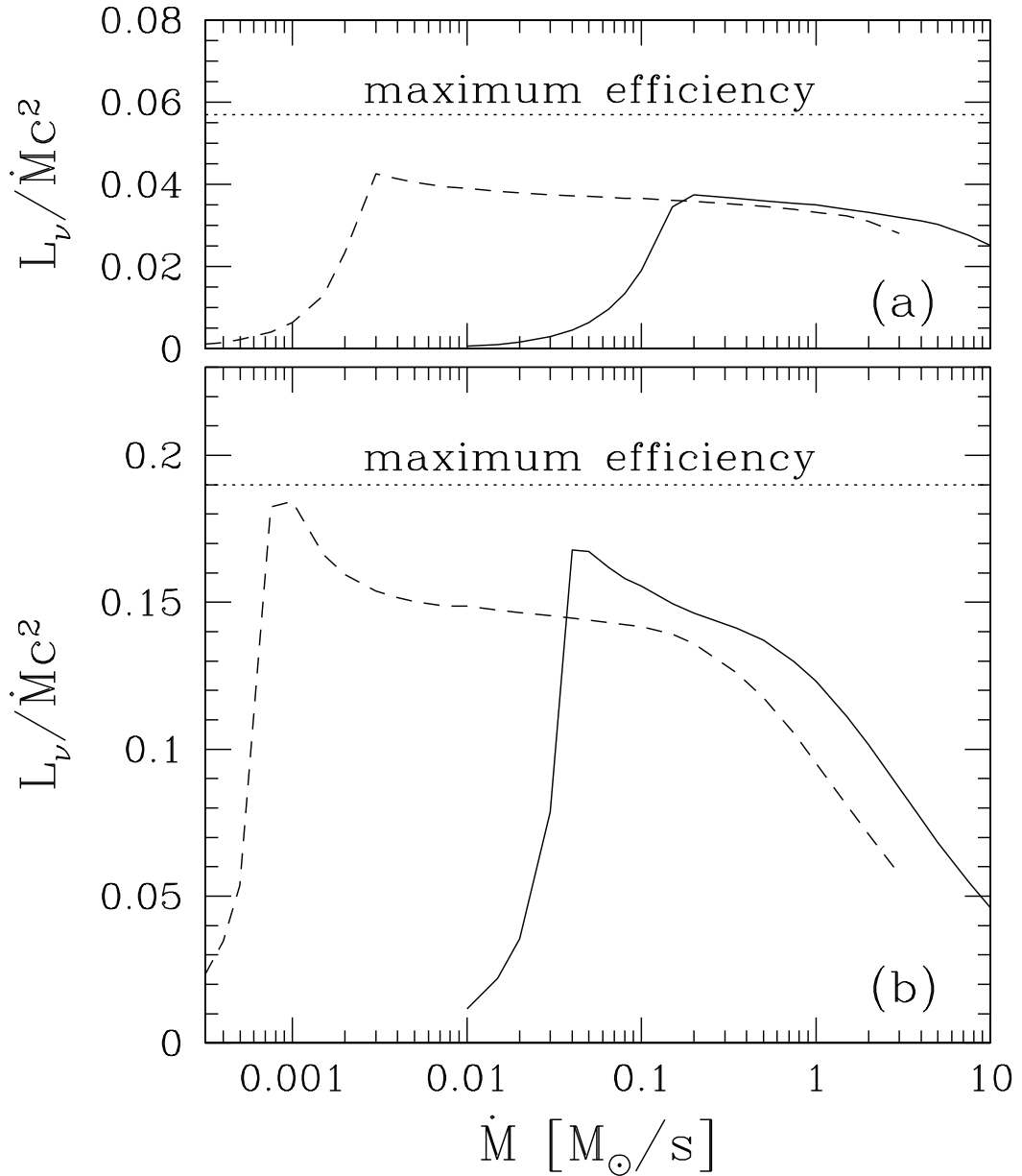


Fig. 18.— Net efficiency of neutrino cooling of the disk $L_\nu/\dot{M}c^2$. The cases of $\alpha = 0.1$ and $\alpha = 0.01$ are shown by the solid and dashed curves, respectively. The maximum efficiency that corresponds to complete cooling is shown by the horizontal dotted curve. (a) Schwarzschild disk ($a = 0$). (b) Kerr disk ($a = 0.95$).